NASA TECHNICAL NOTE

NASA TN D-7979

4.

STRAIN-GAGE BRIDGE CALIBRATION AND FLIGHT LOADS MEASUREMENTS ON A LOW-ASPECT-RATIO THIN WING

Ellwood L. Peele and Clinton V. Eckstrom

Langley Research Center
Hampton, Va. 23665

3.

NATIONAL AERONAUTICS AND SPACE ADMINISTRATION • WASHINGTON, D. C. • OCTOBER 1975

5.

1. Report No.	2. Government Accession No.	3. Recipient's Catalog No.
NASA TN D-7979		

4. Title and Subtitle

STRAIN-GAGE BRIDGE CALIBRATION AND FLIGHT LOADS MEASUREMENTS ON A LOW-ASPECT-RATIO THIN WING

5. Report Date: October 1975

6. Performing Organization Code

7. Author(s)

Ellwood L. Peele and Clinton V. Eckstrom

8. Performing Organization Report No.: L-9896

9. Performing Organization Name and Address

NASA Langley Research Center
Hampton, Va. 23665

10. Work Unit No.: 505-02-22-01

11. Contract or Grant No.

12. Sponsoring Agency Name and Address

National Aeronautics and Space Administration
Washington, D.C. 20546

13. Type of Report and Period Covered: Technical Note

14. Sponsoring Agency Code

15. Supplementary Notes

16. Abstract

Strain-gage bridges were used to make in-flight measurements of bending moment, shear, and torque loads on a low-aspect-ratio, thin, swept wing having a full depth honeycomb sandwich type structure. Standard regression analysis techniques were employed in the calibration of the strain bridges. Comparison of the measured loads with theoretical loads are included.

17. Key Words (Suggested by Author(s))

Flight loads
Strain-gage calibration

18. Distribution Statement

Unclassified – Unlimited

Subject Category 02

19. Security Classif. (of this report)	20. Security Classif. (of this page)	21. No. of Pages	22. Price*
Unclassified	Unclassified	53	$4.25

*For sale by the National Technical Information Service, Springfield, Virginia 22161

STRAIN-GAGE BRIDGE CALIBRATION AND FLIGHT LOADS MEASUREMENTS ON A LOW-ASPECT-RATIO THIN WING

Ellwood L. Peele and Clinton V. Eckstrom
Langley Research Center

SUMMARY

A low-aspect-ratio, thin, swept wing of stainless steel skin-aluminum alloy honeycomb core sandwich construction (i.e., no internal spars or ribs) was instrumented with three strain-gage bridges attached to the outer skin surfaces and an additional bridge located on a vertical face at the wing crossover section. Both point and multipoint calibration loads were applied at selected locations on the wing and the bridge responses were recorded. Standard regression analysis techniques were used to calculate load coefficients for equations giving bending moment, torque, and shear loads at a section near the wing root. Eight sets of load coefficients were established by using various combinations of calibration loads and by deleting one or more bridges in an effort to establish a statistically reliable loads equation. A flight test was conducted and bridge outputs were measured for various maneuver conditions at both subsonic and supersonic airspeeds. Measured flight loads were determined using all eight sets of load coefficients. These results are presented and are compared with theoretical calculations of the loads based on analytically determined pressure distributions.

To explore possible improvements from a larger number of bridges and a different orientation, a loads calibration study was made on a vertical fin structure that was similar in planform and construction to that of the main wing. The vertical fin had eight strain-gage bridges located on the outer skin surface along a chordline parallel to and near the root section. The relationship of load coefficients and probable error was slightly improved by the use of additional bridges and the changes in orientation.

INTRODUCTION

Loads resulting from airflow over the external surfaces of a structure are generally determined either directly from measurements of surface pressure at numerous locations on the structure or indirectly from measurements of strain at selected locations on the structure. If pressure measurements are used, the distribution of pressure loading is obtained. The bending moment, shear, and torque loads can be calculated for any specified location and axis system by integrating the pressure distribution and its

first moments. Techniques for determining loads from strain measurements require an adequate loads calibration procedure and a good choice of locations for taking strain measurements. The loads calibration procedure consists of establishing a relationship between bridge output and applied load. One of the most useful treatments of loads calibration procedures is presented in reference 1. The method presented in reference 1 is based on a regression analysis of a collection of strain-gage bridge outputs obtained from the application of loads in a calibration procedure. In the regression analysis, a load equation is assumed for each type load measurement desired. The equation consists of a summation of the products of the bridge outputs and the coefficients determined from the regression analysis.

The technique of reference 1 has been shown to work very well when applied to aircraft structures with easily determined load paths such as high-aspect-ratio wings with a spar type structure. The problems associated with measuring loads on a low-aspect-ratio vertical fin with a spar-stringer type structure were discussed in references 2 and 3 wherein the techniques of reference 1 were employed with some variations and improvements. This report presents a discussion of the application of the procedures of reference 1 to a low-aspect-ratio, thin, swept wing having a full depth honeycomb core sandwich type construction. This type structure differs from those evaluated in references 1, 2, and 3 in that the full depth honeycomb core contains no structural member, such as a spar, to which the strain-gage bridges could be attached. As a result, a strain-gage bridge exhibiting highly selective shear response was not available. This difficulty, although present to some extent in previous investigations, is more severe for the type of structure inyestigated herein.

Information is presented on the method of instrumenting and calibrating the wing along with a discussion on how the responses of the strain-gage bridges were evaluated in terms of their usefulness for loads prediction. Standard regression analysis techniques were used to calculate bridge output load coefficients for equations giving bending moment, torque, and shear loads at a section near the wing root. Several sets of load coefficients were derived using various combinations of calibration loads and strain-gage bridges in an effort to establish statistically reliable loads equations. A flight test was conducted in which bridge outputs were recorded for various maneuvers and flight conditions at both subsonic and supersonic airspeeds. Measured flight loads were determined using several different sets of load coefficients. These results are compared with calculated theoretical loads based on theoretical pressure distributions.

It should be noted that this flight loads measurement program was initially an add-on to an existing flight-test program. For this reason the number of data channels available and the time allowed for installation and study of the instrumentation limited the scope of the investigation. It is believed that the results presented provide insight into

the problems associated with measuring flight loads on this type of structure, which would be of use to future investigators.

An additional loads calibration study was conducted on a vertical fin similar in planform and construction to that of the wing. The purpose of the study was to determine whether the orientation of the bridges relative to the root chord and the number of bridges employed has a significant effect on the reliability of the derived load coefficients. Results of this study are presented in the appendix.

SYMBOLS

b	fin height, m
c	local streamwise chord, m
F	point calibration load, N
L_i	ith general load (i.e., V, M, and T)
M	moment about X-axis, N·m
$\Delta p/q$	pressure differential/unit dynamic pressure
q	dynamic pressure, N/m^2
S_i	area of ith aerodynamic box, m^2 (fig. 10)
T	torque about Y-axis, N·m
V	shear outboard of $y = 0$, N
X,Y	reference axes (figs. 3 and 13)
x_i	torque arm, m (fig. 10)
x_r	reference x-dimension, 0.127 m
y	distance along Y-axis (table VII and fig. 13)
y_i	moment arm, m (fig. 10)
y_r	reference y-dimension, 0.419 m

α	angle of attack, deg
β_{ij}	coefficients of jth bridge for ith load equation
μ_{ij}	jth bridge output due to application of ith load, mV
μ_{TF}	output of forward torque bridge, mV
μ_{TR}	output of rear torque bridge, mV
μ_{M}	output of moment bridge, mV
μ_{V}	output of shear bridge, mV

WING DESCRIPTION

The low-aspect-ratio, thin, swept wing on which the investigation is based is different than other wings for which structural loads reports are available (refs. 1, 2, and 3). The wing structure consists of upper and lower surfaces of tapered thickness stainless steel bonded to a full depth aluminum honeycomb core. There are no internal spar or rib-like structures used. It is the standard wing for the BQM-34E drone aircraft (supersonic Firebee II). A three-view schematic of the aircraft is shown in figure 1. A photograph of the test wing removed from the aircraft is presented in figure 2. The drone wing has the following physical characteristics and dimensions:

Aspect ratio	2.5
Taper ratio	0.30
Leading-edge sweep angle, deg	53
Maximum thickness, percent of chord length	3
Wing span, m	2.723
Wing reference area, m^2	2.97
Wing net exposed area, m^2	2.15
Wing tip chord, m	0.503

STRAIN-GAGE BRIDGE INSTALLATIONS

With the proper location, orientation, and calibration of strain-gage bridges, a structure such as the drone wing can be used indirectly for measuring bending moment, shear, and torque loads applied to the wing. To achieve this condition, the strain-gage bridges, each consisting of four active arms, must be located and properly oriented at positions

on the structure where the material strain is primarily a function of the type loading it is desired to measure. For this application only four strain-gage bridges were used because of limitations imposed by the overall flight-test operation. One of these bridges was intended primarily for the measurement of shear, one for bending moment, and two for torque loads. The two bridges intended for the measurement of torque loads are configured to measure shear stress due to torque loads and are referred to hereafter as torque bridges. These strain-gage bridges were located on the wing as shown in figure 3. Normally the shear and bending-moment strain-gage bridges are mounted on the main structural members, i.e., the internal spars. However, the structure of this wing consisted only of upper and lower tapered stainless steel surfaces bonded to a full depth aluminum honeycomb core. Therefore, it was necessary to mount all the strain gages on the external surfaces of the wing. A photograph showing the two torque bridges and the upper half of the bending-moment bridge mounted on the outer surface of the upper wing skin is presented in figure 4. The shear-type strain gage was located on a vertical surface in the wing crossover section as was shown in figure 3. The strain gages used were micro-measurement type with gage factors of $2.095 \pm \frac{1}{2}$ percent.

The reference axis system and the strain-gage bridges are usually located either parallel to the aircraft center line or perpendicular to the wing-sweep axis as in reference 1. For this investigation the reference axes were oriented parallel to and perpendicular to the wing 40-percent chordline for the following reasons: (1) vibration tests performed by the wing manufacturer indicated that the wing could be assumed to respond to transverse loads like a beam with an elastic axis located at approximately the 40-percent chordline and (2) the predicted shift in chordwise center of pressure with Mach number (to be discussed later) would result in a change in the sign of the measured torque. The one bending moment and two torque bridges used were therefore located and oriented with respect to the 40-percent chordline as shown in figure 3. It was assumed that with these bridges oriented with respect to and near the elastic axis, the bending-moment bridge would be primarily responsive to bending-moment loads and relatively independent of torque loads and the converse would be true for the torque-type bridges. These assumptions were later determined to have been reasonably valid.

As shown in figure 3, a shear-type bridge was also used but it was located away from the axis system on a vertical surface where the wing structure is carried across the fuselage area. Although this is referred to as a shear-type bridge, it was later determined to be sensitive to bending moment and torque, as well as shear, and therefore was not a useful shear bridge.

Program constraints on time available for installation and evaluation of the strain-gage bridges prior to a series of scheduled flight tests precluded any possible changes in the number of bridges, bridge locations, or orientations to find arrangements more suitable in terms of both magnitude and character of the bridge responses.

CALIBRATION PROCEDURE

The calibration procedure of reference 1 was used in this investigation and is based on the assumption that a relationship exists whereby the structural loads for shear V, bending moment M, and torque T are given in terms of a linear combination of the bridge outputs. For example, the load equation for the ith load type L_i at a given spanwise station is

$$L_i = \beta_{ij}\mu_j$$

where the load coefficients β_{ij} relate the load L_i to the bridge outputs μ_j. Values for the load coefficients are determined for each ith load and jth bridge by applying transverse calibration loads to the structure and recording the bridge outputs μ_{ij}. The load and bridge outputs are written in matrix notation as an equation

$$\langle L \rangle = [\mu]\langle \beta \rangle$$

If the number of calibration loads exceeds the number of bridges, a solution for the coefficients can be obtained by a least-squares curve fit procedure (i.e., a regression analysis) which in matrix notation is

$$\langle \beta \rangle = \left([\mu]^T[\mu]\right)^{-1}[\mu]^T\langle L \rangle$$

where the superscript T denotes matrix transposition and the superscript -1 denotes matrix inversion. Except for the meaningless case where all gage outputs are identical $\left(\text{which leads to a singular matrix } \left([\mu]^T[\mu]^{-1}\right)\right)$, a solution will always be found for the coefficients β_{ij}. However, it is not always certain that the β_{ij} coefficients will lead to reliable load determinations.

Calibration Loadings and Bridge Outputs

The electrical output of each of the four strain-gage bridges was recorded for both the point loads and multipoint loads applied to the wing at the locations shown in figure 5. In order that the calibration loads (inert weights) produce stresses similar in direction to upward steady flight loads, the wing was inverted but supported in the same manner as it is when attached to the drone aircraft. Sponge rubber pads, 0.05 m × 0.05 m (2 in. × 2 in.) were placed between the inert weights and the wing surface to avoid high local stress concentrations.

Two calibrations were performed, one prior to and one following the flight test. Applied loads were limited to a maximum of 356 N (80 lb) for the first calibration because it was essential that the calibration procedure would in no way damage the wing or jeopardize its usefulness for the flight test. Later, it was questioned whether the loads applied during the first calibration were large enough to eliminate any possible nonlinear response at low load values. The second calibration was conducted in essentially the same manner as the first except that the point loads were increased to a maximum of 890 N (200 lb) and the combined total of multipoint loads to 3560 N (800 lb). For the second calibration, load points 6, 7, and 10 were omitted because of difficulty in applying the loads.

For both calibrations, the bridges were excited with a regulated 5-volt dc power supply. Calibration loads were applied in 25-percent increments from zero to the maximum value. Examples of strain-gage bridge outputs for both the first and second calibrations are shown in figure 6. Note that the scale is different for the output of the forward torque bridge. The outputs of both the forward torque bridge and the aft torque bridge were low in magnitude. From the examples shown in figure 6 it can be seen that there were no significant changes in the linearity or slopes of the bridge outputs when the higher calibrate loads were applied during the second calibration.

For the point-load calibrations a straight line was fitted to the calibration data by the least-squares method. The slope of this line was then used to calculate the bridge output for the maximum loading wherein it was assumed that the bridge output should be zero for zero load. These calculated bridge output values are presented in tables I and II along with the calibration loading and the associated bending moment, shear, and torque loads for the first and second calibrations, respectively.

It should be pointed out that the bending moment, shear, and torque loads depend on the set of reference axes chosen. Different values would be calculated for different axis systems. As shown in tables I and II (for loads applied at points 1, 4, 7, and 10), the assumption was made that shear load at the reference axis was zero. The same assumption was made for loads applied at points 1, 2, and 3 with regard to torque. The calibration loading procedure was changed for the vertical tail discussed in the appendix so that all calibrate load points were located outboard of the bridges being evaluated.

Discussion of Bridge Output

The responses or outputs of the strain-gage bridges to the calibration loads were evaluated in terms of their usefulness for loads prediction on the following three points: (1) linearity of the bridge outputs with respect to the amplitude of the applied load, (2) the capability to superimpose the bridge outputs from the point loads to match the outputs from the multipoint loadings, and (3) ability of the bridge to discriminate between load types, i.e., bending moment, shear, and torque.

Linearity of bridge output versus applied load.- For small deformations, most conventional aircraft structures respond linearly with applied load. Strain bridge output which is proportional to local strain should likewise be linear. The bridge outputs μ_{ij} exhibited a linear relationship with applied load as seen in the examples shown in figure 6. The degree of linearity did not change significantly between the first and second calibrations.

Superposition of bridge outputs.- For the principle of superposition to apply, it should be possible to synthesize the bridge response to a combination of simultaneously applied point loads from the response of the bridge to independently applied point loads. The principle was tested by analytically combining the appropriate bridge outputs from several different point loads and comparing the result with the bridge response to loads applied simultaneously to the same points. The results are shown in figure 7, along with a listing of what multipoint loads were used. Note that the bridge output scales are different and that the output from the torque bridges is very small. As can be seen, the response of the forward torque bridge was quite similar in shape and magnitude for both the multipoint load calibration and the summation of the point load calibration data. The rear torque bridge response, however, was considerably different for the multipoint loading than for the summation of the point load data. The response of the bending-moment bridge was nearly the same for the multipoint load and the summation of data for the point load data. The response of the shear bridge was similar for both multipoint load and point load data through the second step in the multipoint loading process. Thereafter the shear bridge output due to the multipoint load was significantly less than the summation of the appropriate point load data. The principle of superposition appears to be valid for the bending-moment bridge but only partially valid for the forward and rear torque and the shear bridges.

Bridge load discrimination.- The capability of a strain-gage bridge to discriminate between load types, i.e., bending moment, shear, or torque can be determined qualitatively by examining the change in bridge output per unit load as a function of a change in the moment arms for constant torque arms and the reverse. These quantities, referred to as influence coefficients, are presented in figures 8 and 9 for the first and second calibrations, respectively. The influence coefficients are calculated using the values of bridge outputs and point loads given in tables I and II. In figures 8(a) and 9(a) the influence coefficients are presented as a function of the spanwise location of the applied load with the chordwise location as a parameter. In figures 8(b) and 9(b) the same influence coefficients are presented, this time as a function of the chordwise location of the applied load with the spanwise location as a parameter. In general, if the parametric curves are nearly coincident, independence of a variation in that parameter is indicated. Figures 8 and 9 show

that the torque bridges have the desired dominant response to the chordwise location of the applied load, although they are not completely independent of the spanwise location. The bending-moment bridge has the best response in that its output per unit loading is very sensitive to the spanwise location of the applied load and relatively insensitive to the chordwise location. The shear bridge exhibits a combined sensitivity to bending moment, shear, and torque. The shear bridge output is sensitive to the spanwise and chordwise location of the applied load; whereas, it should give a constant output for a constant magnitude load, independent of the location of its application.

Figures 8 and 9 also show that the influence coefficients are essentially the same for both the first and the second calibrations, as would be expected from examination of figure 6. It is believed that the differences between the first and second calibrations are primarily an indication of the accuracy with which the point loads can be applied rather than an indication of a change in sensitivity due to higher applied loads for the second calibration. Because the inert weights used for the second calibration were physically much larger than the rubber pads on which they were placed, some small differences in the exact location of the applied load could easily exist. This may be the cause of the differences in the bending-moment bridge influence coefficients for load point 1. Load point 1 was at the same location as the bending-moment bridge; and, for this reason, the output response would be extremely dependent on the exact location of the applied load. Load points 6, 7, and 10 were not included in the second calibration because of difficulty in applying the loads.

Load Coefficients and Probable Errors

In an effort to develop statistically reliable loads equations, load coefficients based on eight different combinations of bridges and/or calibration loads were established as follows:

Set no.	Calibration number	Point loads	Multipoint loads	Bridge output used			
				μ_{TF}	μ_{TR}	μ_{M}	μ_{V}
1	1	13		X	X	X	X
2	1	10		X	X	X	X
3	2	10		X	X	X	X
4	2	10	4	X	X	X	X
5	2		10	X	X	X	X
6	2		10	X	X	X	
7	2		10	X		X	X
8	2		10	X		X	

Statistical theory provides two numbers which are useful in evaluating the reliability of the regression equations (at least in determining the loads on which they are based). They are the estimate of probable error for the calculated structural load and the estimate of probable error in each load coefficient. The average calibration loading (bending moment, shear, or torque) on which each set of load coefficients is based is presented in table III along with the probable error of estimate of load for each set. The probable errors of estimate for the various loadings range from 1 to 17 percent of the average applied shear loading, 1 to 23 percent for torsion, and 1 to 4 percent for moment. Set 5, which uses all four bridges and is based on multipoint calibrate loading data, provides the most statistically reliable equations for determining all the load components, although sets 6 and 7 also appear to be good for torque, and sets 2, 6, 7, and 8 for moment. It was suggested in reference 1, for load coefficients where the probable error of the coefficient was large in comparison with the coefficient, that the associated bridge outputs should be omitted from the load equation as being irrelevant. Furthermore, for bridges with similar, i.e., linearly related, influence coefficient plots, the output from all but one bridge should be discarded because of redundancy. If the number of available bridges is small, however, as is the case here, the omission of gages may not be practical.

All the eight different sets of load coefficients were used to calculate flight loads (discussed in a later section) in order to determine the effect that the differences in statistical accuracy of the load equations have on the resulting derived flight-loads data.

THEORETICAL AERODYNAMIC LOADS CALCULATIONS

Drone wing aerodynamic pressure distributions per unit dynamic pressure which result from a steady spanwise uniform angle of attack were calculated for Mach numbers 0.8 and 1.2 and several angles of attack. The calculations were made using the computer program described in reference 4. Wing-body interference effects were included for a circular cylinder of constant diameter through the wing section. The aerodynamic box layout of the wing and the simplified representation of the fuselage are shown in figure 10.

The theoretical pressure distributions for the wing at the various flight conditions are presented in table IV for angles of attack of 0° and 1°. The pressure $\left(\Delta p/q\right)_i$ which was assumed constant over each individual box was multiplied by the respective box area S_i and moment arm x_i or y_i if appropriate, and then summed over all boxes outboard of the reference X-axis to obtain bending moment, shear, and torque. The contribution to bending moment, shear, and torque of the boxes through which the X-axis passed was made proportional to the percentage of their area outboard of the X-axis. The following expressions were employed:

$$V = \sum_i \left(\frac{\Delta p}{q}\right)_i S_i$$

$$M = \sum_i \left(\frac{\Delta p}{q}\right)_i S_i y_i$$

$$T = \sum_i \left(\frac{\Delta p}{q}\right)_i S_i x_i$$

where $(\Delta p/q)_i$, S_i, x_i, and y_i are the pressure differential per unit dynamic pressure, the area, the torque arm, and the moment arm of the ith box. (See fig. 10.) These equations do not include inertial effects due to acceleration factors since inertia effects for this wing are very small. The values of theoretical wing loads determined by the above equations are given in table V as a function of angle of attack for two Mach numbers. Note that the sign of the theoretical wing torque loading changes as the Mach number changes from 0.8 to 1.2. This results from a shift of the center of pressure from ahead of to behind the 40-percent chordline of the wing.

FLIGHT LOADS MEASUREMENTS

The instrumented wing was flight tested on a Navy BQM-34E drone aircraft by the Naval Missile Center, Point Mugu, California. A total of 18 flight conditions were selected for investigation, of which 6 were for straight and level, steady flight and the remaining 12 flight conditions were for quasi-steady maneuvers. The straight- and level-flight conditions were performed to obtain data at specified Mach numbers and angle-of-attack conditions. The quasi-steady maneuvers included sustained high g turns at vertical load factors of 2g, 3g, and 5g and a series of pullups from dives which produced maximum vertical load factors of approximately 2g. The maneuvers were performed over a wide range of altitude and Mach number conditions. A listing of the test parameters for each of the 18 test points evaluated is presented in table VI, along with a listing of outputs of the four wing-mounted strain bridges. A listing of the estimated accuracy of the flight data measurements is given at the bottom of table VI. The external fuel tank (see fig. 1) was released from the aircraft after the first eight of the test points.

Two checks of the strain-gage-bridge circuits were performed during the flight test. These checks were accomplished by a command signal which caused a calibration resistor to be shunted into one arm of each bridge circuit. The resulting change in bridge output provided an indication that the bridge circuits were intact and that they were receiving an excitation voltage of the correct magnitude.

COMPARISON OF MEASURED AND THEORETICAL LOADS

The eight sets of load coefficients presented in table III were used with the bridge outputs of table VI to determine the flight-test structural loads for bending moment, shear, and torque. These loads, derived from bridge outputs and load coefficients, are referred to hereafter as measured loads. The measured loads are presented in figure 11 as the ratio of load to the dynamic pressure and as a function of the measured angle of attack for each of three different flight conditions. The flight conditions are: (1) subsonic flight (Mach numbers from 0.86 to 0.96) with the external fuel tank attached to the aircraft fuselage, (2) subsonic flight with the external fuel tank off, and (3) supersonic flight (Mach numbers from 1.06 to 1.18) with the external fuel tank off. The subsonic data are separated into tank-on and tank-off categories to show that the presence of the external fuel tank had a noticeable effect on the measured moment loads. The appropriate theoretically determined loads from table V for subsonic flight (Mach number, 0.8) or supersonic flight (Mach number, 1.2) are also shown in figure 11 for comparison purposes. The external fuel tank was not included in the theoretical representation of the aircraft. Therefore the possible interference between the external tank and the wing surface was not accounted for. The measured loads (V, T, and M) are presented for each of the eight different sets of load coefficients to show what effect, if any, the use of different calibrate procedures or the use of different combinations of bridges had on the resulting measured flight loads.

Shear Loads

The shear loads measured during the flight test and the theoretically determined shear loads are shown in figures 11(a), 11(b), and 11(c). For the subsonic tank-on and the supersonic tank-off flight conditions, the shear loads measured using the first six sets of load coefficients show considerable scatter (figs. 11(a) and 11(b)), although there is reasonable agreement with the theoretical values. The shear loads measured using the last two sets of load coefficients show considerably less scatter for both flight conditions.

For the subsonic tank-on flight condition (fig. 11(a)), it can be seen that for most sets of data the measured shear loads are less than the theoretically determined shear loads. This is to be expected since an increase in angle of attack of about 1° is required to maintain the same total aircraft lift when the external fuel tank is in place. For the supersonic tank-off flight condition (fig. 11(b)), the measured shear loads are in fair agreement with the theoretically determined values, particularly as evidenced by sets 7 and 8 which have less scatter in the measured data. For the subsonic tank-off flight condition (fig. 11(c)), the measured shear loads show less scatter and fair agreement with the theoretically determined values for all eight sets of load coefficients.

It was indicated earlier that the eight sets of load coefficients were defined in an effort to establish a statistically reliable loads equation. Referring to the subsonic tank-on flight condition (fig. 11(a)), it can be seen that there is only a small difference in the shear loads measured using load coefficient sets 1 and 2 or sets 3, 4, 5, and 6. Load coefficient sets 1 and 2 are based on using all four bridges and the first calibration point loads only. Load coefficient sets 3, 4, and 5 are based on using all four bridges and the second calibration data. Set 3 is based on point loads only, set 4 on a combination of point loads and multipoint loads, and set 5 on multipoint loads only. Set 6 is based on using only three bridges (omitting the shear bridge) and the second calibration multipoint loading data. The measured data from load coefficient set 5, which had by far the lowest estimate of probable error of load (see table III), is not noticeably different from the measurements based on load coefficient sets 3 and 4.

Load coefficient set 6, which was based on the same set of calibrate loads as set 5 but eliminated the shear bridge, resulted in a slight increase in scatter of the measured data. The shear loads measured using load coefficient sets 7 and 8 show considerable less scatter than those from sets 1 to 6. The rear torque bridge was excluded from consideration for both of these sets of coefficients with the shear bridge also being excluded from set 8. Although the statistical reliability of these two sets of coefficients was much less than that of set 5, the results appear to be considerably improved. Similar reductions in scatter were observed when either the forward or rear torque bridge was excluded from consideration with point load calibrate data. Shear load coefficient set 8 is unique in that the load coefficient for the forward torque bridge is near zero (irrevelant); therefore, the shear loads measured are proportional to the output of the moment bridge only. From figures 8 and 9 it is evident that the output of the moment bridge is a linear function of the applied moment. This result indicates that the shear measurements made by using coefficient set 8 are directly proportional to moment which would preclude any possible determination of a shift in spanwise center of pressure.

Torque Loads

The measured wing torque loads T/q are presented in figures 11(d), 11(e), and 11(f) for the three flight-test conditions. Note that for all flight conditions very low values of torque were measured; although, in most instances, the measured data are of a larger magnitude than the theoretically determined values. For subsonic flight with the external fuel tank on, the measured torque loads (fig. 11(d)) are positive and of a slightly larger magnitude than the theoretically determined values. Positive values of torque indicate the resultant center of pressure is ahead of the 40-percent chordline of the wing. For subsonic flight with the external fuel tank off (fig. 11(f)), there appears to be a slight decrease in the magnitude of the torque loads although they are still positive and of greater magnitude than the theoretical values. For both subsonic flight conditions (external fuel

tank on and off), there is no significant change in the measured data between the various sets of load coefficients.

For supersonic flight, the theoretical calculations (fig. 11(e)) indicated the torque loads would be slightly negative, i.e., the wing center of pressure would be slightly aft of the 40-percent chordline. Measured data for load coefficient sets 1 to 6 indicate slightly positive torque loads; however, for load coefficient sets 7 and 8, the measured torque loads are either near zero or negative in sign and in close agreement with the theoretical values. The primary difference between load coefficient sets 1 to 6 and sets 7 and 8 was that sets 7 and 8 used input measurements from only one of the two torque bridges.

Moment Loads

The flight measurements of moment load M/q are presented in figures 11(g), 11(h), and 11(i). The data have little scatter and agree quite well with the theoretically determined values except for the aircraft tank-on configuration at subsonic speed. The aircraft tank-on data are displaced about 1° in angle of attack from the theoretical line which, as mentioned previously, might be expected since the aircraft must assume about a 1° higher angle of attack to maintain level flight when the external fuel tank is on.

CONCLUDING REMARKS

Flight measurements of bending moment, shear, and torque loads were made on a low-aspect-ratio, thin, swept wing of full depth honeycomb core construction using strain-gage bridges mounted externally on the wing surface.

The wing was calibrated using both point and multipoint loading procedures. Standard regression analysis techniques were used to calculate load coefficients for equations giving bending moment, torque, and shear loads for an axis system located parallel and perpendicular to the 40-percent chordline of the wing with the origin near the wing root. Eight sets of load coefficients were established by using various combinations of calibration loads and by deleting one or more strain-gage bridges.

Several statistically reliable equations for bending-moment loads were developed. This success resulted from having a strain-gage bridge on the wing whose output was primarily responsive to bending-moment loads and essentially independent of variations in shear and torque loads. Statistically reliable equations for shear and torque loads were obtained only when multipoint load calibration data were used in the regression analysis. This was so even though the two strain-gage bridges installed on the wing to measure torque had the desired dominant response to torque loads, although the response was not completely independent of bending-moment loads. The wing, because of its construction, had no internal vertical web suitable for mounting a bridge primarily responsive to shear.

A shear bridge mounted externally on a vertical face at the wing root was used, but it was responsive to variations in torque and moment load as well as shear load. It was conjectured that the capability to measure shear loads on this type structure would be improved if a strain-gage bridge installation more selectively sensitive to shear loads could be devised.

Values of bending moment, derived from flight data using the various sets of load coefficients, consistently gave the same result for each of the flight conditions, exhibited little scatter, and were in excellent agreement with theoretical predictions. Some shear load measurements have considerable scatter; but, in most instances, the measured data showed reasonable agreement with the theoretical values. The torque measurements generally were of slightly larger magnitude than the theoretical values, although both the theoretical and measured values of torque loads were very low. The measured torque loads generally indicated the wing center of pressure was slightly ahead of the theoretically predicted locations for subsonic flight and showed a slight rearward shift for supersonic flight. There was no obvious correlation between statistical accuracy of the loads equations and scatter in the measured flight loads data, particularly for the shear and moment measurements.

The relationship of load coefficients and probable error was improved slightly by using a larger number of strain-gage bridges and changing the orientation of the reference axis system.

Langley Research Center
National Aeronautics and Space Administration
Hampton, Va., 23665
June 11, 1975

APPENDIX

VERTICAL-TAIL LOADS CALIBRATION STUDY

The experience gained with the low-aspect-ratio, thin, swept wing discussed in the main text of this report, along with information presented in references 2 and 3 (a loads investigation on a low-aspect-ratio vertical tail), indicated that there might be advantages to using a larger number of strain-gage bridges and a reference axis system alined parallel and perpendicular to the aircraft longitudinal axis. Subsequently, a vertical fin similar in planform and construction to that of the flight-test wing was instrumented with eight strain-gage bridges at four locations near the fin root and mounted as shown in figure 12. Calibration load application points are shown in figure 13 along with the strain-gage bridge locations and the reference axis system. Note that four of the strain-gage bridges (5, 6, 7, and 8) were installed in the bending-moment bridge configuration, and the remaining four bridges (1, 2, 3, and 4) were installed in the torque bridge configuration with one bridge of each type being at each of the four locations. Calibration loading values and corresponding strain-gage bridge outputs are listed in table VII.

Influence coefficients were determined and plotted as a function of spanwise location of the applied load with the chordwise location as a parameter, and as a function of chordwise location of the applied load with the spanwise location as a parameter, as was done with the wing. The plots are shown for each bridge in figure 14. The bridges were mounted with the intention they either respond primarily to bending moment or to torque. Observe from figure 14(a) that bridges 1, 7, 8, and possibly 6, appear to be good bending-moment bridges; whereas, bridges 6, 7, and 8 were designed to respond to bending moment and bridge 1 to torque. The sensitivity of bridge 1 is small compared with the others and probably would not be useful. Further, observe from figure 14(b) that bridges 2, 3, 5, and possibly 4, appear to be good torque bridges. It is interesting to note that the bridges at forward locations 1 and 5 have reversed their functions. This may be due to distortion of load paths in this area. Thus, a moment about the X-axis would not necessarily result in the principal stress acting in the y-direction. A comparison of the influence coefficient plots for the fin in figure 14 with those for the wing presented in the main body of the report (figs. 8 and 9) indicates no significant improvement in bridge load discrimination from the change in orientation.

Load coefficients for bending moment, shear, and torque load equations were calculated for the axis system shown in figure 13. All bridge outputs and all load points were included in the regression analysis. The resulting coefficients and the associated probable errors are listed in table VIII. The orientation and the number of bridges used on the

vertical tail provided a slight overall improvement in the relationship between the coefficients and their probable errors over those obtained for the bridge arrangement of the test wing.

Five different combinations of bridges were employed in each of which several bridges were omitted. The best results were obtained when all the bridges were used.

REFERENCES

1. Skopinski, T. H.; Aiken, William S., Jr.; and Huston, Wilber B.: Calibration of Strain-Gage Installations in Aircraft Structures for the Measurement of Flight Loads. NACA Rep. 1178, 1954. (Supersedes NACA TN 2993.)

2. Havell, P. B.; Webber, D. A.; and Roberts, T. A.: The Interpretation of Strain Measurements for Flight Load Determination. CP No. 839, British A.R.C., 1966.

3. Havell, P. B.; Webber, D. A.; and Roberts, T. A.: The Use of Calibrated Strain Gauges for Flight Load Determination. CP No. 1041, British A.R.C., 1969.

4. Carmichael, Ralph L.; Castellano, Charles R.; and Chen, Chuan F.: The Use of Finite Element Methods for Predicting the Aerodynamics of Wing-Body Combinations. Analytic Methods in Aircraft Aerodynamics, NASA SP-228, 1970, pp. 37-51.

TABLE I.- CALIBRATION LOADS, WING LOADING, AND BRIDGE OUTPUTS – FIRST CALIBRATION

Load point	Calibration load, N	Wing loading			Bridge output, mV			
		Shear, N	Torque, N·m	Moment, N·m	μ_{TF}	μ_{TR}	μ_{V}	μ_{M}
1	358	0	0	0	1.56×10^2	1.75×10^2	37.75×10^2	-0.74×10^2
2	↓	358	0	150	2.80	4.42	97.70	27.90
3		358	0	300	1.59	6.78	154.70	56.63
4		0	45	0	3.00	4.09	32.60	.92
5		358	45	150	6.51	8.82	85.70	27.75
6		358	45	300	5.47	12.40	143.30	56.88
7		0	-45	0	.21	-.41	46.10	1.42
8		358	-45	150	-1.17	-1.54	107.50	26.94
9		358	-45	300	-2.39	1.02	66.00	55.71
10		0	-90	0	-.92	-3.75	166.80	2.39
11		358	-90	150	-4.43	-7.61	122.10	25.94
12		358	-90	300	-6.41	-4.88	178.00	55.35
13		358	-136	150	-7.35	-13.60	136.00	24.92

TABLE II.- CALIBRATION LOADS, WING LOADING, AND BRIDGE OUTPUTS – SECOND CALIBRATION

Load point	Calibration load, N	Wing loading			Bridge output, mV			
		Shear, N	Torque, N·m	Moment, N·m	μ_{TF}	μ_{TR}	μ_V	μ_M
1	890	0	0	0	5.36×10^2	5.68×10^2	1.03	-0.158
2	↓	890	0	373	8.34	11.46	2.39	.729
3		890	0	746	6.10	17.20	3.70	1.462
4		0	113	0	11.90	11.42	.94	.489
5		890	113	373	19.60	24.46	2.22	.722
6	---	---	----	---	----------	----------	----	------
7	---	---	----	---	----------	----------	----	------
8	890	890	-113	373	-1.70	-3.90	2.62	.709
9	890	890	-113	746	-5.22	1.08	3.90	1.439
10	---	---	----	---	----------	----------	----	-----
11	890	890	-226	373	-9.70	-17.90	2.82	.685
12	890	890	-226	746	-14.36	-11.76	4.10	1.436
13	890	890	-339	373	-17.60	-32.84	2.95	.648

TABLE III.- SUMMARY OF LOAD COEFFICIENTS AND PROBABLE ERRORS

Equation for –	Set no.	Average wing calibration loading, N	Probable error of load estimate, N	Load coefficients ± probable errors			
				$\beta_{V,TF}$, N/mV	$\beta_{V,TR}$, N/mV	$\beta_{V,M}$, N/mV	$\beta_{V,V}$, N/mV
V	1	246	±41	9124 ± 1450	-6294 ± 1009	1540 ± 238	-130 ± 61
	2	285	±34	8765 ± 1286	-5780 ± 906	1242 ± 250	-35 ± 66
	3	712	±123	6668 ± 1648	-4663 ± 1172	925 ± 274	3 ± 83
	4	1334	±94	5693 ± 774	-3941 ± 525	771 ± 133	44 ± 45
	5	2180	±19	4998 ± 523	-3167 ± 411	545 ± 45	131 ± 19
	6	2180	±39	8201 ± 467	-5773 ± 309	854 ± 6	Omitted
	7	2180	±43	1023 ± 189	Omitted	225 ± 40	269 ± 16
	8	2180	±182	0.12 ± 756	Omitted	900 ± 25	Omitted
		N·m	N·m	$\beta_{T,TF}$, N·m/mV	$\beta_{T,TR}$, N·m/mV	$\beta_{T,M}$, N·m/mV	$\beta_{T,V}$, N·m/mV
T	1	52	±12.2	346 ± 430	470 ± 299	107 ± 70	-60 ± 18
	2	50	±6.3	-47 ± 235	826 ± 166	-77 ± 46	-7 ± 12
	3	124	±15.7	213 ± 211	627 ± 150	1 ± 35	-32 ± 11
	4	214	±12.3	67 ± 122	742 ± 83	-24 ± 21	-25 ± 7
	5	260	±1.7	-90 ± 45	751 ± 36	-5 ± 4	-32 ± 2
	6	260	±8.6	866 ± 103	1382 ± 68	-80 ± 1	Omitted
	7	260	±9.4	852 ± 41	Omitted	71 ± 9	-64 ± 3
	8	260	±43.5	1097 ± 181	Omitted	-91 ± 6	Omitted
		N·m	N·m	$\beta_{M,TF}$, N·m/mV	$\beta_{M,TR}$, N·m/mV	$\beta_{M,M}$, N·m/mV	$\beta_{M,V}$, N·m/mV
M	1	150	±4.1	349 ± 145	-319 ± 101	602 ± 24	-16 ± 6
	2	164	±1.6	233 ± 60	-215 ± 42	-215 ± 42	2 ± 3
	3	410	±15.3	-500 ± 204	325 ± 145	369 ± 34	47 ± 10
	4	746	±14.8	-276 ± 101	164 ± 69	405 ± 17	38 ± 6
	5	1267	±4.3	-210 ± 117	119 ± 92	470 ± 10	15 ± 4
	6	1267	±5.6	153 ± 67	-177 ± 44	505 ± 1	Omitted
	7	1267	±4.2	-61 ± 18	Omitted	482 ± 4	10 ± 2
	8	1267	±7.5	-98 ± 31	Omitted	507 ± 1	Omitted

TABLE IV.- THEORETICAL WING PRESSURE DISTRIBUTION $\Delta p/q$

[See fig. 10(b)]

Mach number, 0.8								
Spanwise location	Chordwise location –				Chordwise location –			
	1	2	3	4	1	2	3	4
	$\alpha = 0^o$				$\alpha = 1^o$			
1	-0.00927	-0.00545	-0.01048	-0.00541	0.06305	0.05486	0.02741	0.01807
2	-.00375	-.00515	-.00645	-.00377	.08497	.04810	.03087	.01815
3	-.00453	-.00415	-.00396	-.00223	.09572	.05200	.03350	.01867
4	-.00462	-.00365	-.00289	-.00151	.10540	.05559	.03494	.01858
5	-.00459	-.00310	-.00225	-.00117	.11438	.05906	.03578	.01796
6	-.00450	-.00271	-.00178	-.00091	.12291	.06186	.03569	.01669
7	-.00433	-.00238	-.00142	-.00068	.13069	.06315	.03360	.01431
8	-.00408	-.00200	-.00105	-.00047	.13594	.06011	.02742	.01049
9	-.00353	-.00131	-.00058	-.00025	.12947	.04208	.01553	.00555

Mach number, 1.2								
Spanwise location	Chordwise location –				Chordwise location –			
	1	2	3	4	1	2	3	4
	$\alpha = 0^o$				$\alpha = 1^o$			
1	0.002114	0.003625	-0.019312	-0.01733	0.05836	0.05297	0.02760	0.02863
2	-.00127	-.00284	-.00954	-.01263	.07165	.04962	.03941	.03433
3	-.00251	-.00496	-.00695	-.00944	.08358	.05201	.04455	.03898
4	-.00361	-.00588	-.00848	-.00447	.09471	.05671	.04567	.04588
5	-.00435	-.00670	-.00684	-.00373	.10637	.06223	.05099	.04723
6	-.00504	-.00734	-.00588	-.00277	.11905	.06863	.05565	.04517
7	-.00593	-.00757	-.00512	-.00139	.13307	.07592	.05764	.03373
8	-.00840	-.00602	-.00362	-.00008	.14714	.08274	.04354	.01877
9	-.00926	-.00354	-.00179	-.00106	.15950	.05132	.02049	.00769

TABLE V.- THEORETICAL WING LOADS

Mach number	α, deg	V/q, N/N/m^2	M/q, N·m/N/m^2	T/q, N·m/N/m^2
0.8	1	0.039	0.0195	0.00073
	2	.081	.0400	.00123
	5	.206	.1014	.00274
1.2	1	0.048	0.0260	-0.00138
	2	.102	.0543	-.00363
	5	.264	.1390	-.01040

TABLE VI.- FLIGHT-TEST PARAMETERS AND BRIDGE OUTPUTS

Test point	Test maneuver	Mach number, M	Altitude, km	Aircraft weight		Vertical load factor, g units	Dynamic pressure, q		Angle of attack α, deg	Bridge outputs, mV			
				N	lbf		N/m^2	lb/ft^2		μ_{TF}	μ_{TR}	μ_M	μ_V
1	Pull up	0.92	*0.40	9821	2208	1.85	5.74×10^4	1200	2.40	1.55	1.45	2.60	4.0
2	Cruise	.80	*.55	9334	2166	.90	4.29	895	1.85	.75	.70	1.75	1.6
3	Cruise	.85	*1.35	9412	2116	.90	4.44	925	1.80	.75	.95	1.85	1.6
4	Right turn	.85	*1.40	9327	2097	3.05	4.40	920	4.80	1.45	1.70	6.20	12.0
5	Cruise	.90	2.30	9056	2036	.95	4.57	955	1.70	.80	1.15	1.50	-.7
6	Cruise	.94	5.00	8829	1985	1.00	3.62	755	1.70	.75	1.20	1.35	1.9
7	Left turn	.86	5.05	8660	1947	2.95	2.96	620	6.00	.95	1.45	5.90	11.8
8	Climb	.86	7.95	8478	1906	.85	2.15	450	2.80	.30	.70	1.85	1.8
9	Pull up	1.07	10.60	8020	1803	1.70	2.31	480	2.95	.20	.70	3.85	9.2
10	Cruise	1.06	10.95	7966	1791	.95	2.12	445	1.35	.05	.50	2.25	4.2
11	Left turn	1.08	11.75	7864	1768	2.00	1.97	410	4.10	.33	.70	4.55	10.9
12	Cruise	1.13	11.75	7731	1738	.95	2.03	425	1.60	.10	.30	2.05	3.4
13	Dive	1.18	7.20	7642	1718	.85	4.25	890	.50	.15	.30	1.55	3.3
14	Pull up	1.13	4.80	7624	1714	2.25	5.26	1100	1.50	.55	.50	4.20	9.6
15	Pull up	.94	2.25	7522	1691	2.00	5.11	1070	1.60	.80	.85	3.25	7.1
16	Pull up	.96	2.20	7401	1664	2.00	5.27	1100	1.45	.75	.95	3.25	7.0
17	Pull up	.93	2.75	7925	1640	1.85	4.49	935	1.55	.70	.95	3.05	6.4
18	Right turn	.88	4.45	7152	1608	5.10	3.33	695	6.35	1.10	1.60	8.45	18.9
Estimated accuracies		±0.04	±0.20 ±0.06	±50	±10	±0.20	$\pm 0.12 \times 10^4$	±25	±0.20	±0.20	±0.20	±0.30	±1.0

*Denotes that second estimated accuracy is applicable.

TABLE VII.- VERTICAL-TAIL CALIBRATION LOADINGS AND STRAIN-GAGE BRIDGE OUTPUTS

Load point	Location		Calibration load, N	Bridge output, mV							
				Torque bridges				Moment bridges			
	Percent chordline	y/b		1	2	3	4	5	6	7	8
1	20	0.1	1334	6	-45	-48	-25	-44	-58	-48	-80
2	40	↓	↓	9	6	-19	-2	-14	-53	-49	-68
3	60	↓	↓	11	12	49	32	3	-42	-41	-30
4	80	↓	↓	13	33	88	231	19	-27	-35	202
5	20	0.2	1112	15	-36	-45	-11	-37	-89	-74	-94
6	40	↓	↓	14	5	-10	17	-8	-75	-79	-85
7	60	↓	↓	14	22	51	68	8	-58	-77	-64
8	80	↓	↓	16	41	99	279	23	-42	-72	-3
9	20	0.4	890	20	6	-19	24	-9	-111	-133	-140
10	40	↓	↓	21	23	22	70	4	-97	-136	-140
11	60	↓	↓	21	37	63	143	16	-83	-135	-144
12	80	↓	↓	23	52	104	241	27	-71	-134	-149
13	20	0.6	178	6	6	5	16	1	-28	-42	-46
14	40	↓	↓	6	9	12	28	3	-25	-42	-48
15	60	↓	↓	7	11	18	40	5	-24	-43	-49
16	80	↓	↓	7	14	25	53	8	-21	-43	-50
17	20	0.8	89	4	5	7	17	2	-17	-29	-33
18	40	↓	↓	4	6	10	21	3	-16	-29	-34
19	60	↓	↓	5	8	12	26	3	-15	-29	-34
20	80	↓	↓	5	9	14	30	4	-14	-29	-35

TABLE VIII.- SUMMARY OF LOAD COEFFICIENTS AND PROBABLE ERRORS

Equation for –	Average fin loading	Probable error of estimate	Load coefficients ± Probable errors							
			$\beta_{V,1}$	$\beta_{V,2}$	$\beta_{V,3}$	$\beta_{V,4}$	$\beta_{V,5}$	$\beta_{V,6}$	$\beta_{V,7}$	$\beta_{V,8}$
V	720 N	±48 N	-65.3 ± 16.2	45.3 ± 3.12	20.7 ± 12.9	-1.22 ± 0.46	-83.4 ± 4.9	28.1 ± 3.67	9.69 ± 1.98	1.54 ± 0.038
			$\beta_{T,1}$	$\beta_{T,2}$	$\beta_{T,3}$	$\beta_{T,4}$	$\beta_{T,5}$	$\beta_{T,6}$	$\beta_{T,7}$	$\beta_{T,8}$
T	291 N.m	±7.4 N.m	-5.57 ± 2.5	8.24 ± 0.48	5.98 ± 0.202	-0.163 ± 0.072	-8.71 ± 0.76	-8.31 ± 0.57	3.80 ± 0.31	0.632 ± 0.059
			$\beta_{M,1}$	$\beta_{M,2}$	$\beta_{M,3}$	$\beta_{M,4}$	$\beta_{M,5}$	$\beta_{M,6}$	$\beta_{M,7}$	$\beta_{M,8}$
M	148 N.m	±0.92 N.m	-0.534 ± 0.313	-0.468 ± 0.06	0.230 ± 0.025	0.090 ± 0.009	0.692 ± 0.095	-1.29 ± 0.071	-1.31 ± 0.038	-0.008 ± 0.007

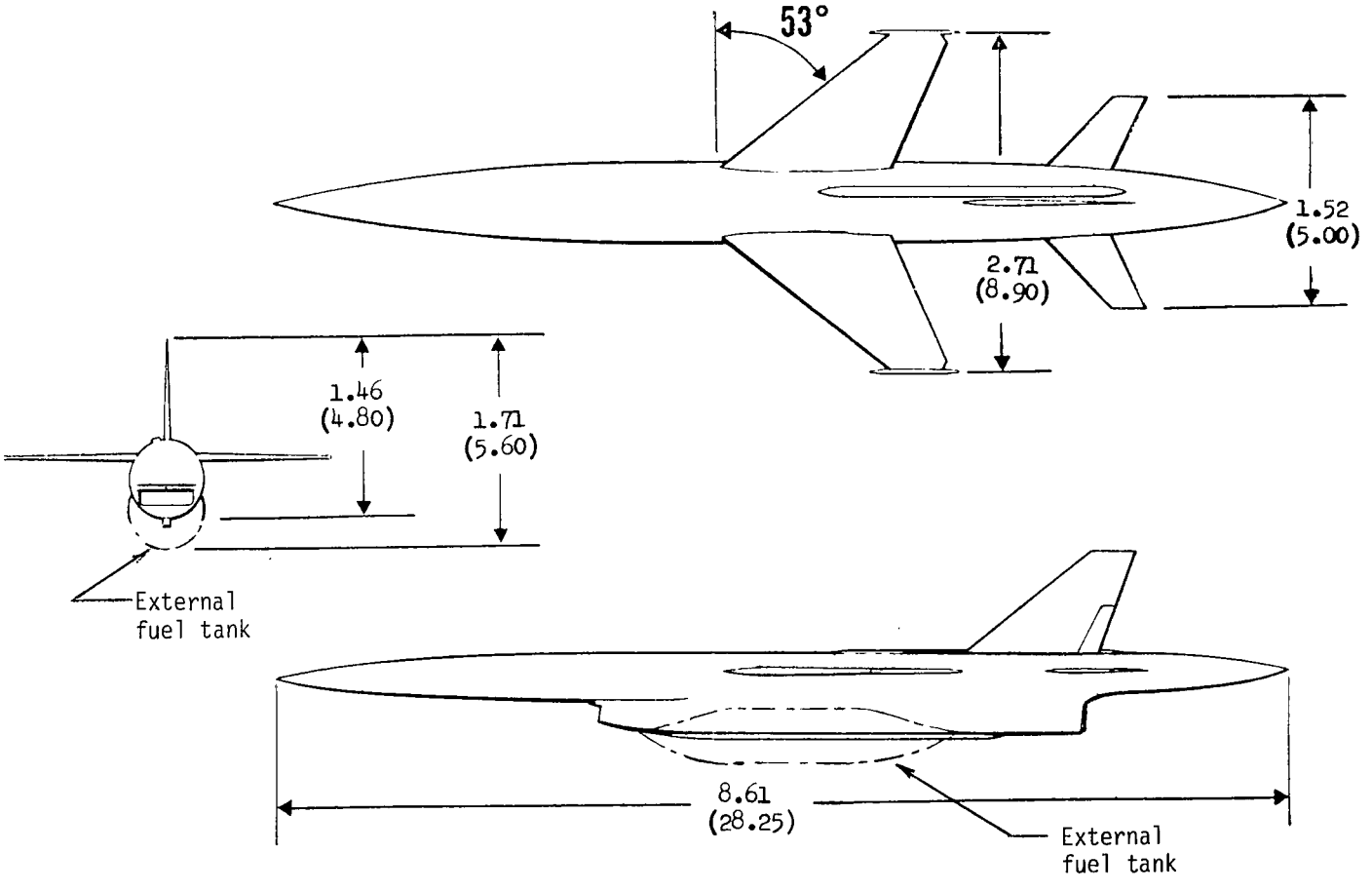

Figure 1.- Three views of test vehicle. Dimensions are in m (ft).

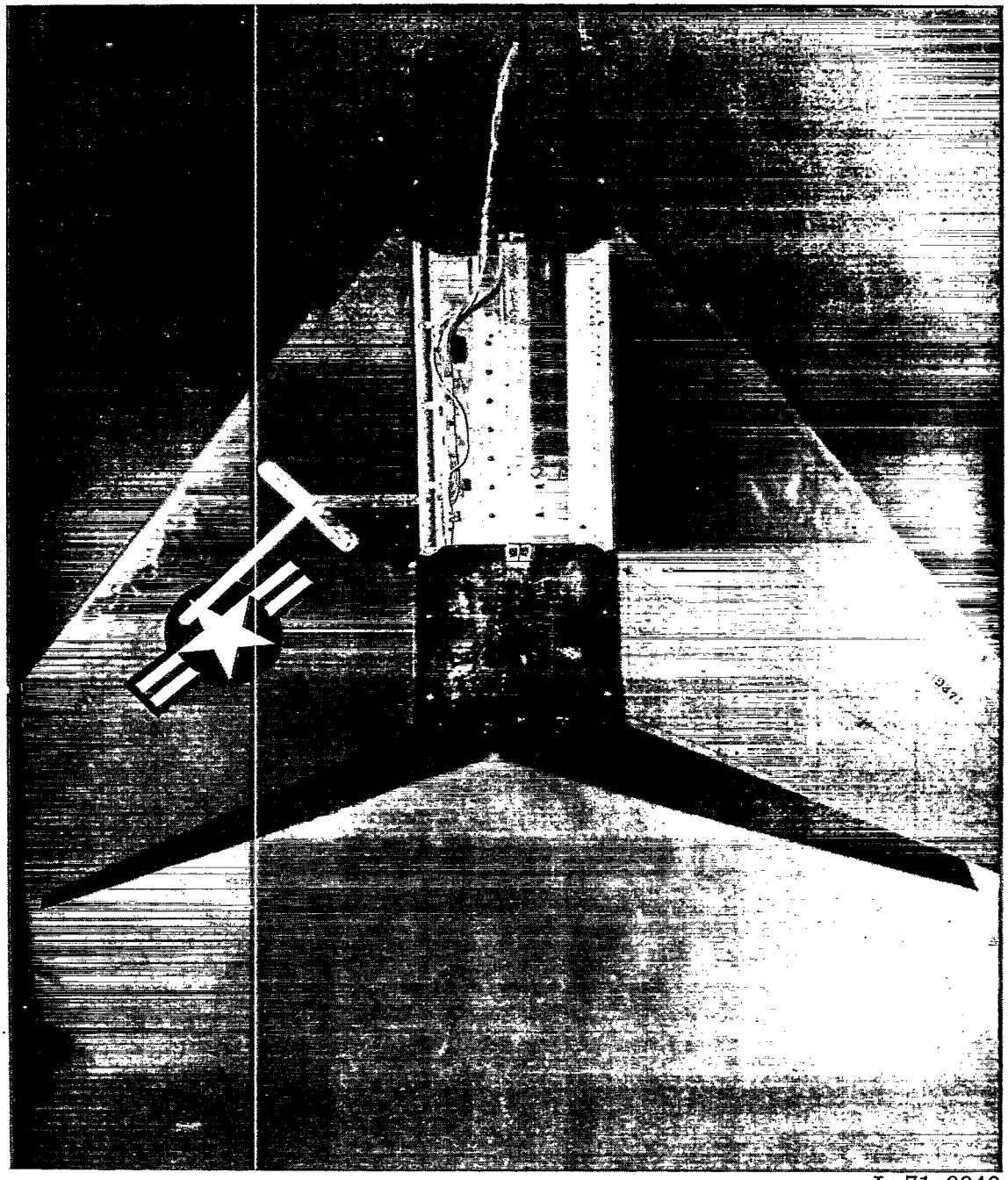

L-71-9949

Figure 2.- Photograph of test wing. (Tips removed.)

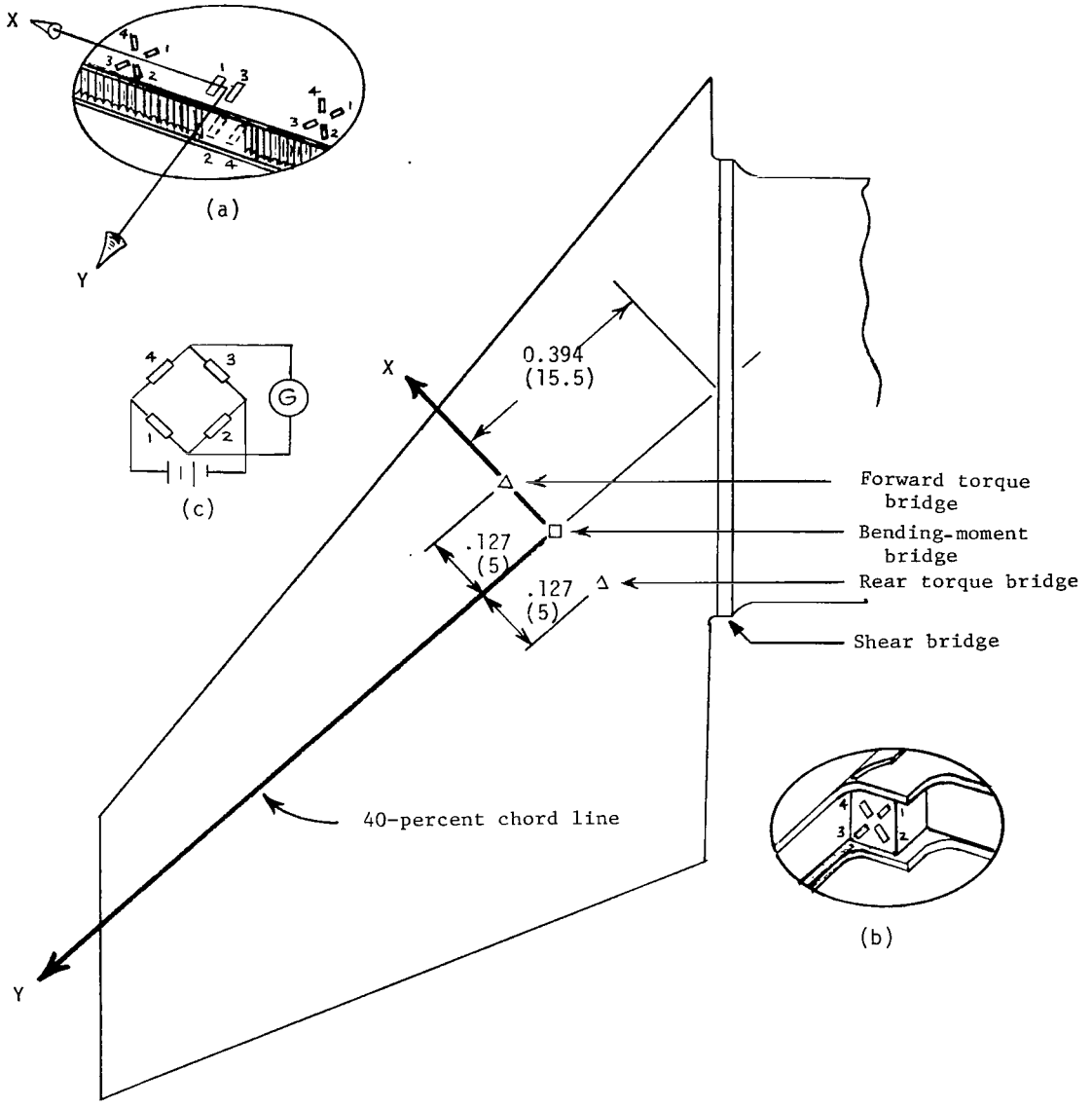

(a) Schematic of bending-moment and torque bridge installations.
(b) Schematic of shear bridge installation.
(c) Circuit diagram for bridge installations.

Figure 3.- Location of strain-gage bridges. Dimensions are in m (in.).

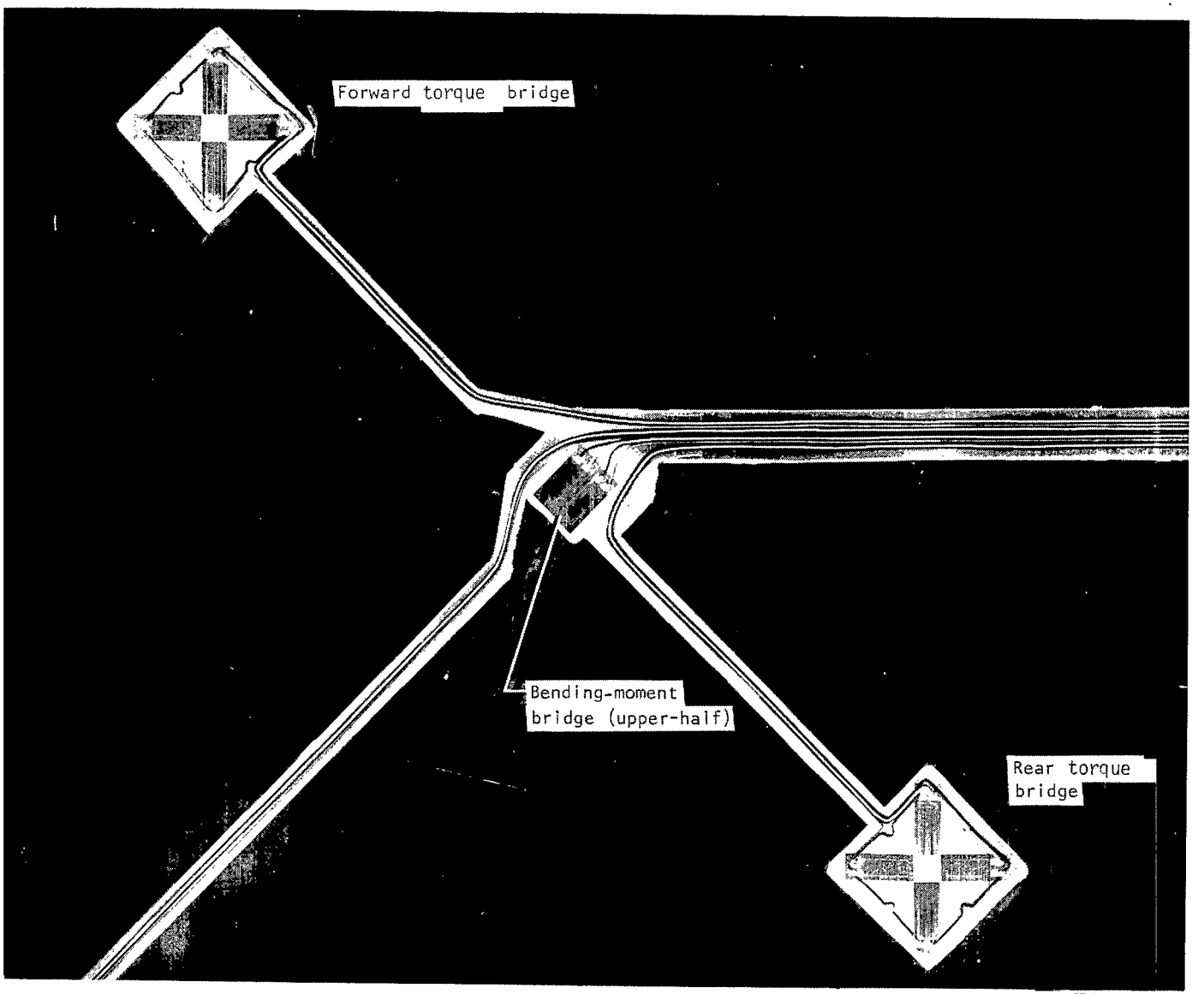

L-71-9367.1

Figure 4.- Photograph showing the strain gages and bridge orientations on the upper surface of the wing.

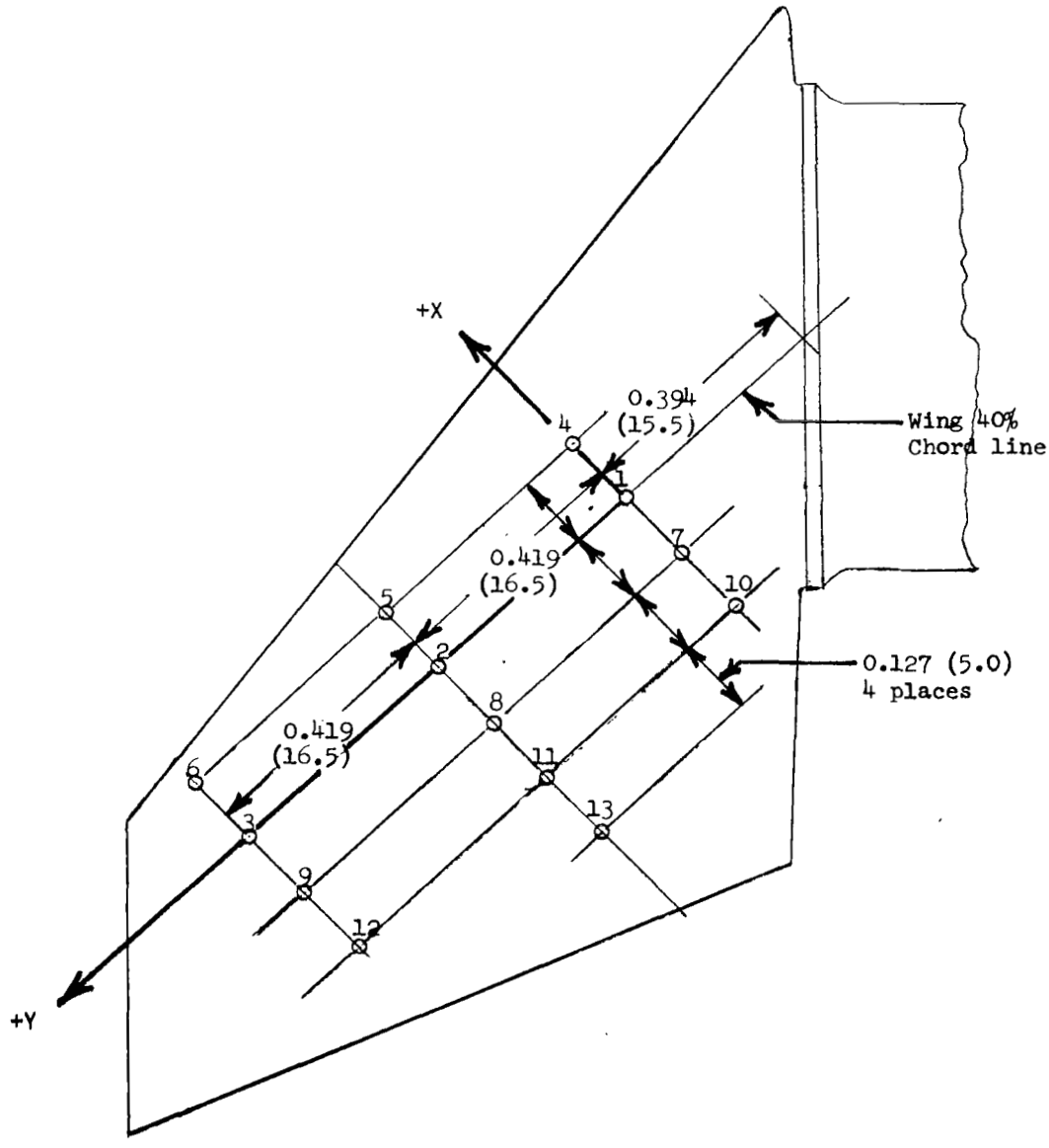

Figure 5.- Calibrate load-point locations. Dimensions are in m (in.).

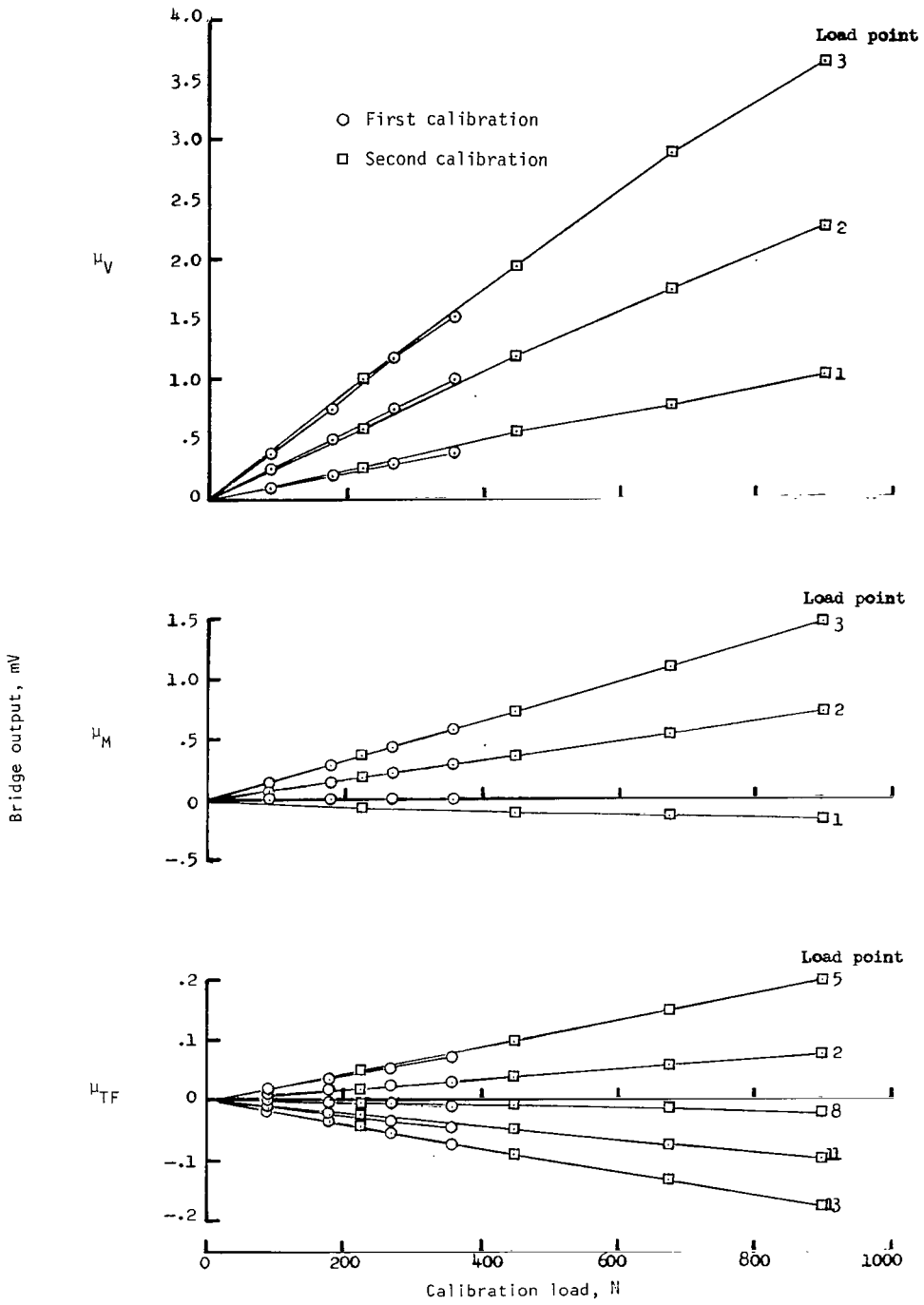

Figure 6.- Examples of strain-gage bridge outputs as a function of calibration load and load location.

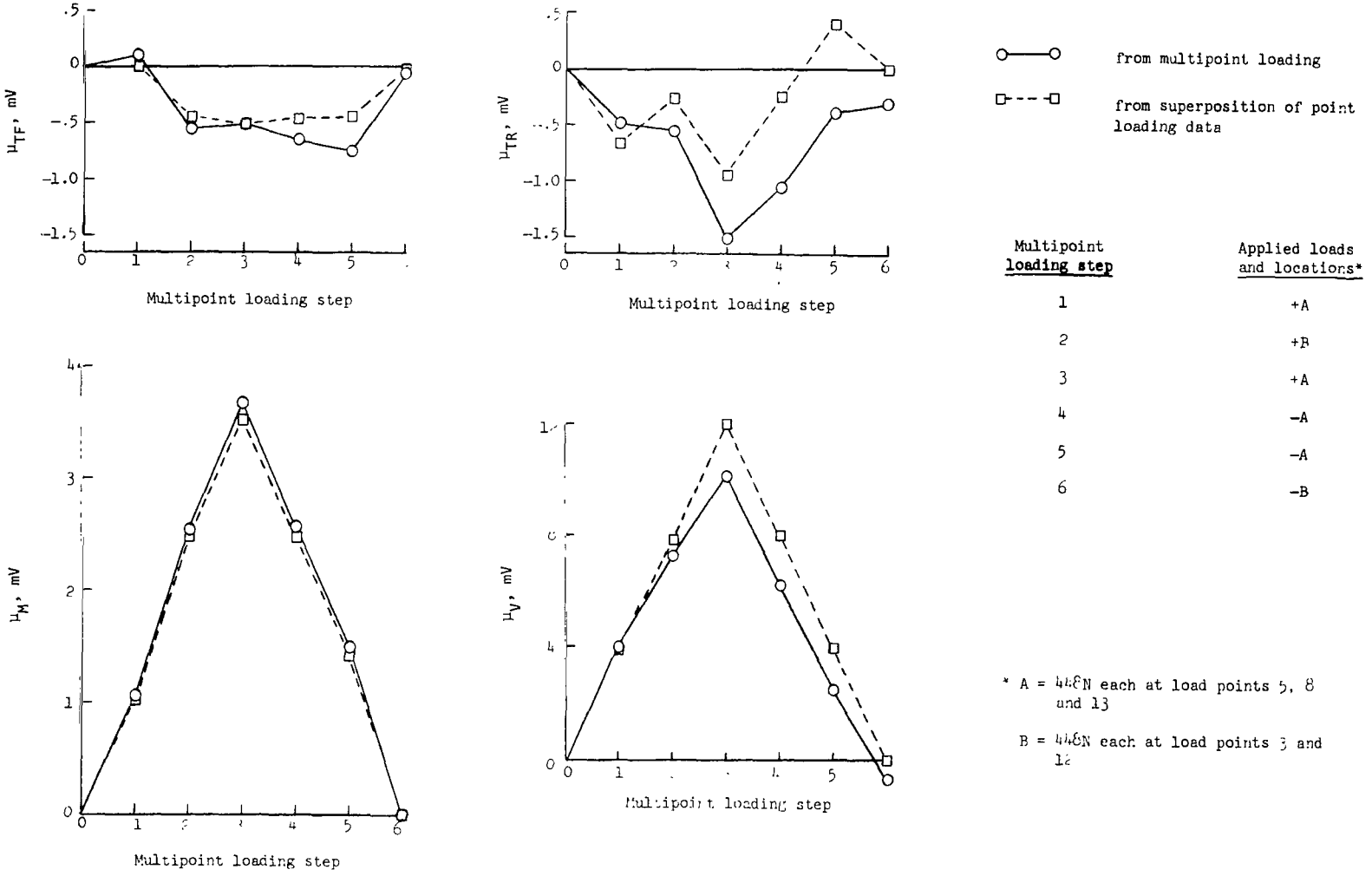

Figure 7.- Comparison of strain-gage bridge response to actual as a function of analytical multipoint loads.

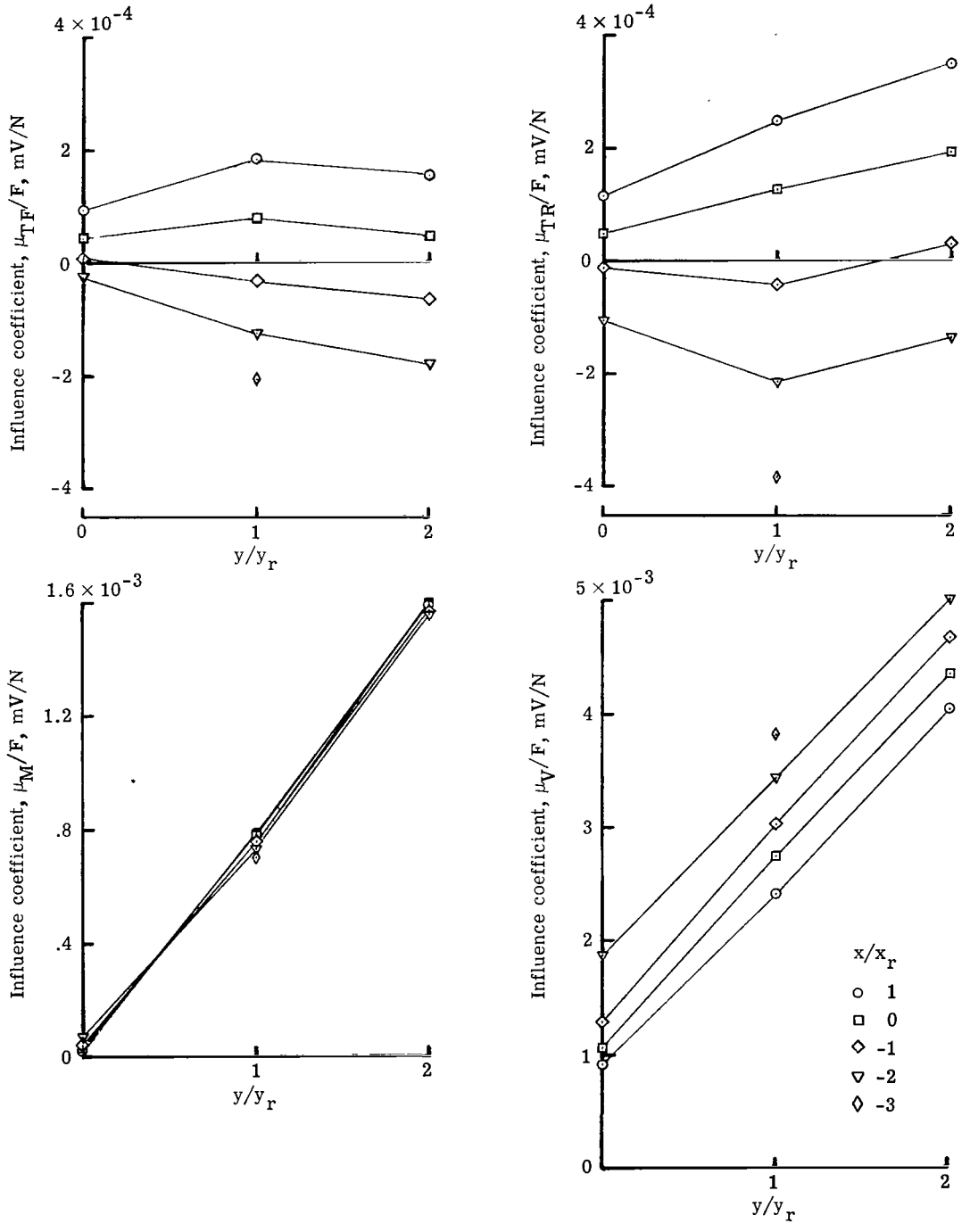

(a) Influence coefficients as a function of y/y_r location of applied point loads.

Figure 8.- Influence coefficients. First calibration.

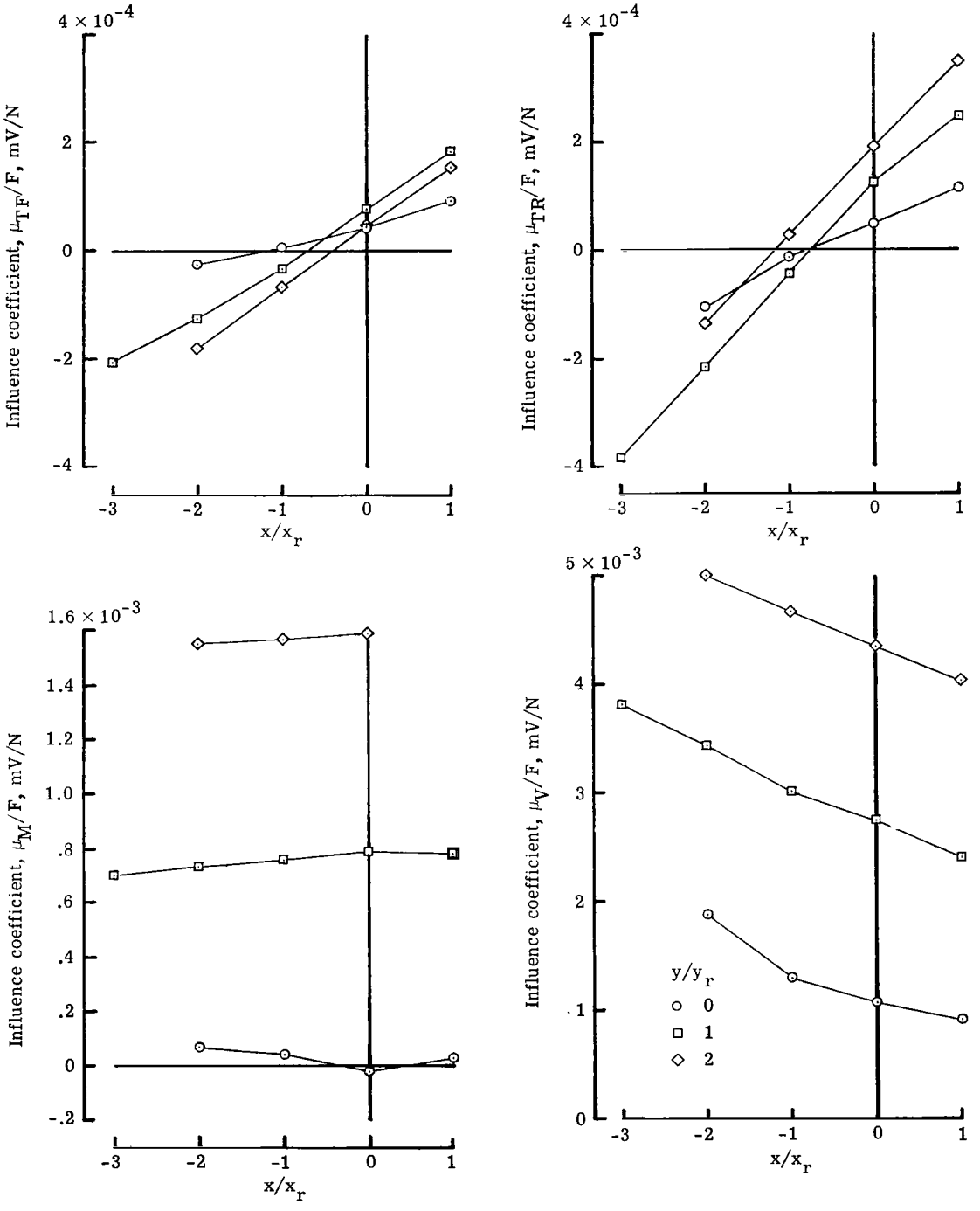

(b) Influence coefficients as a function of x/x_r location of applied point loads.

Figure 8.- Concluded.

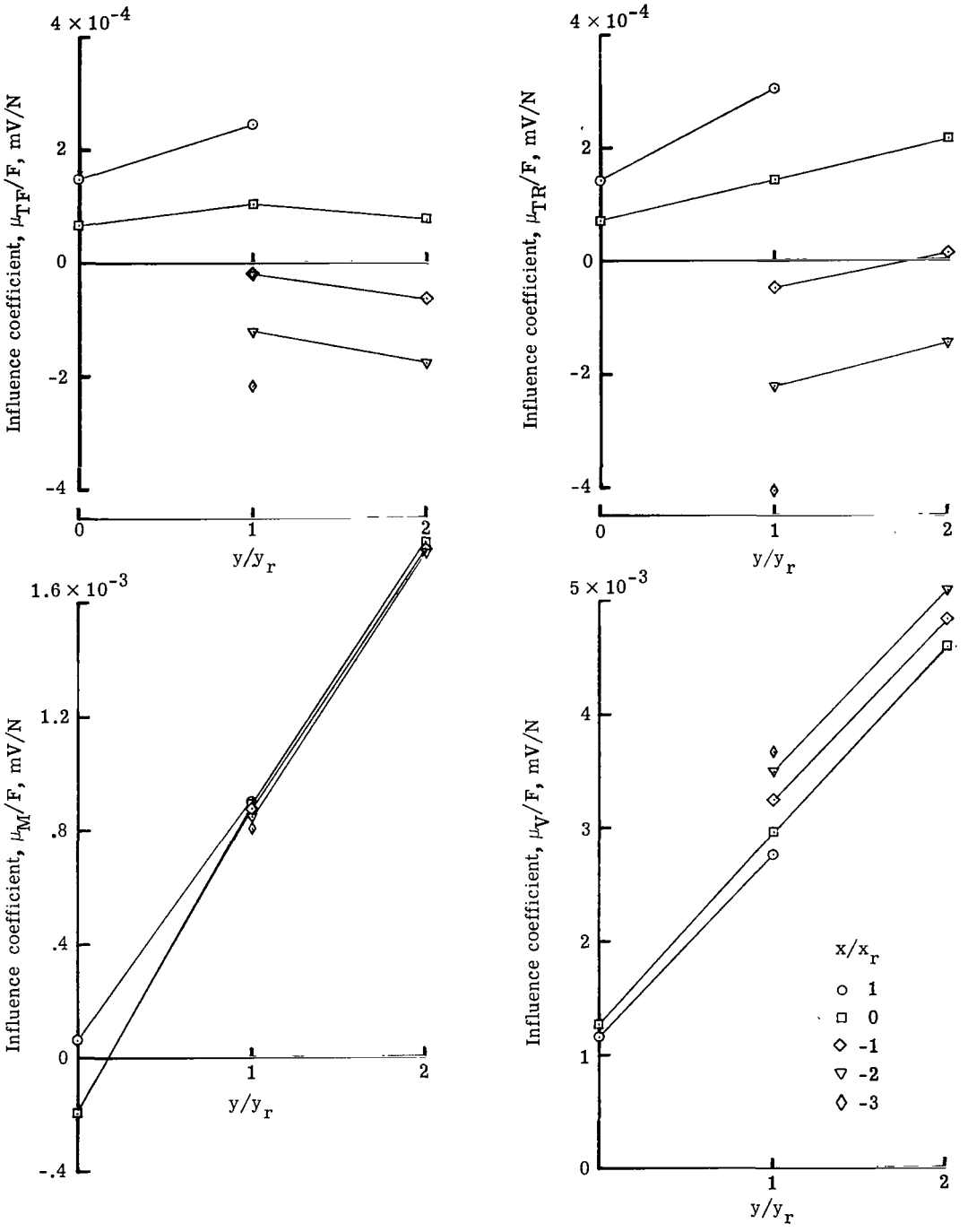

(a) Influence coefficients as a function of y/y_r location of applied point loads.

Figure 9.- Influence coefficients. Second calibration.

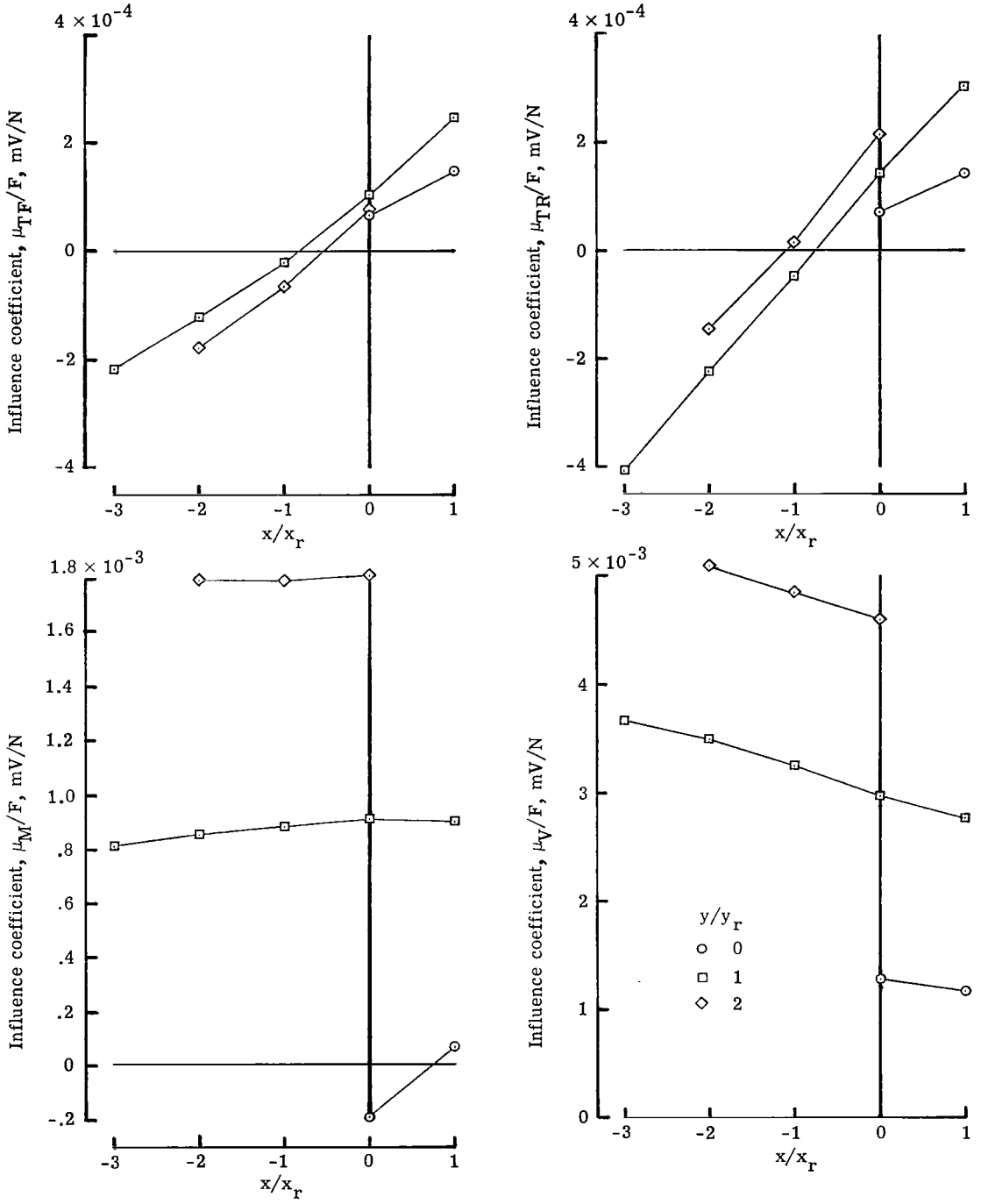

(b) Influence coefficients as a function x/x_r location of applied point loads.

Figure 9.- Concluded.

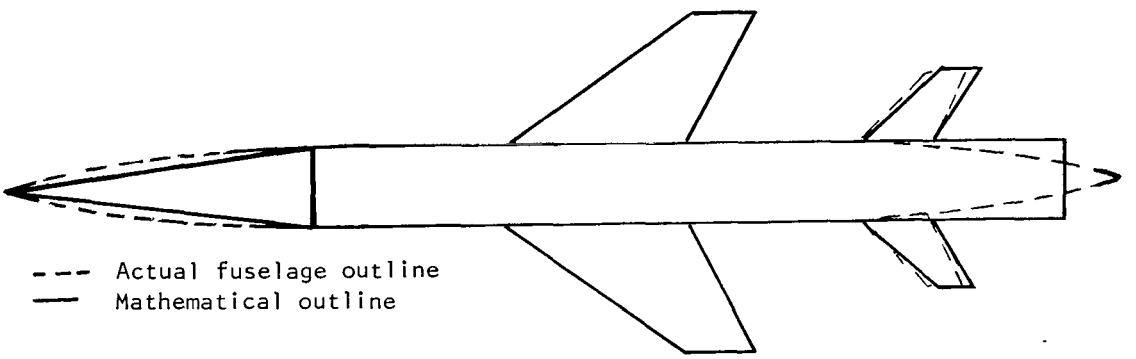

(a) Simplified fuselage representation.

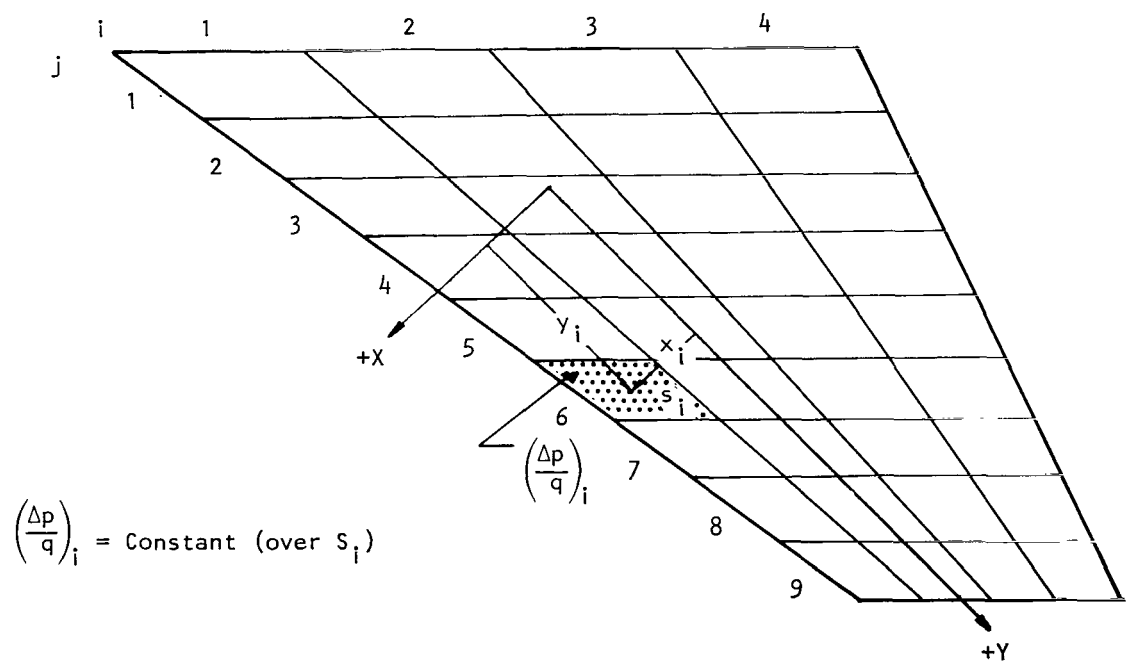

(b) Wing box layout.

Figure 10.- Aerodynamic representation.

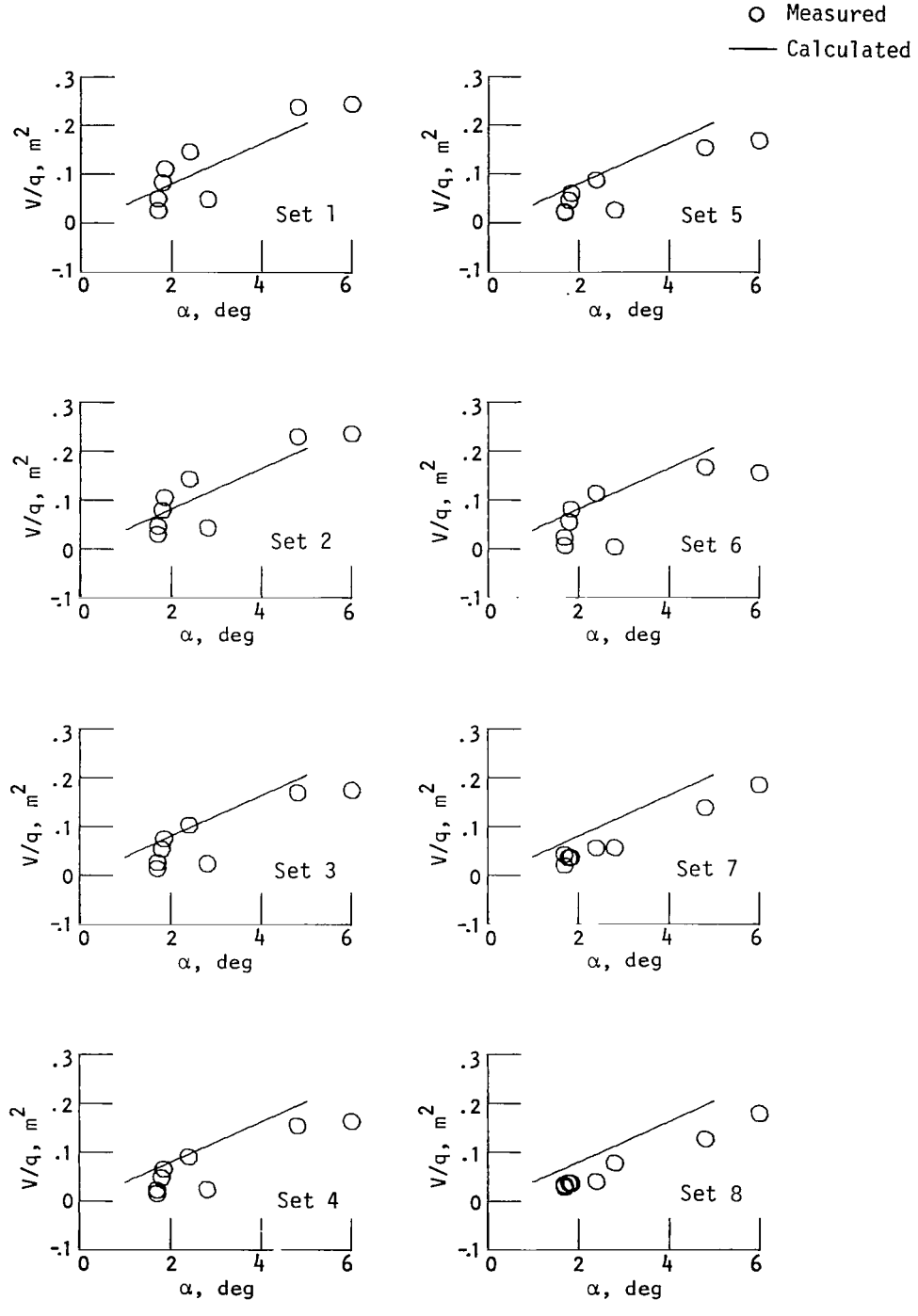

(a) Shear data for subsonic flight, tank-on configuration.

Figure 11.- Comparison of measured and calculated flight loads.

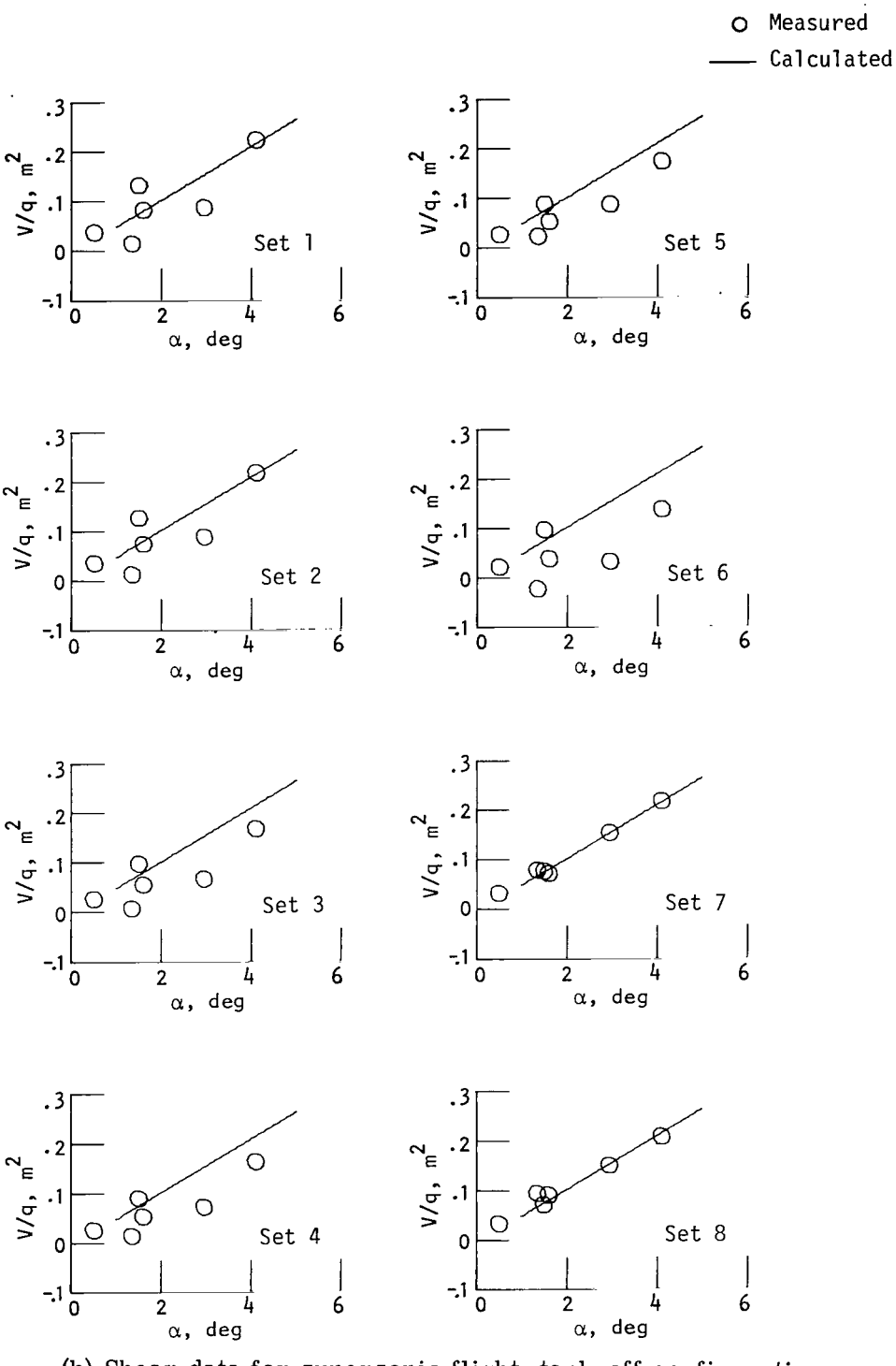

(b) Shear data for supersonic flight, tank-off configuration.

Figure 11.- Continued.

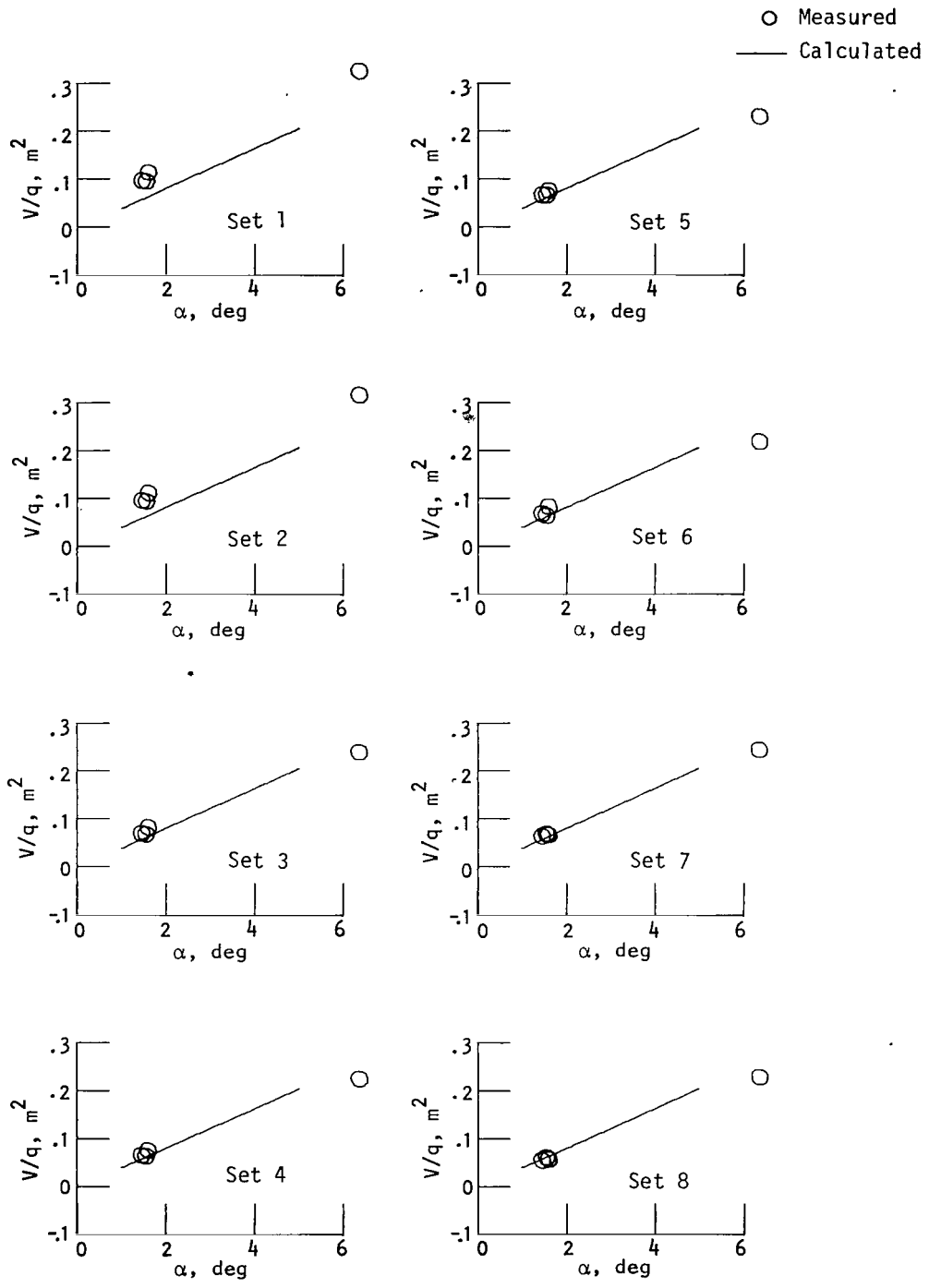

(c) Shear data for subsonic flight, tank-off configuration.

Figure 11.- Continued.

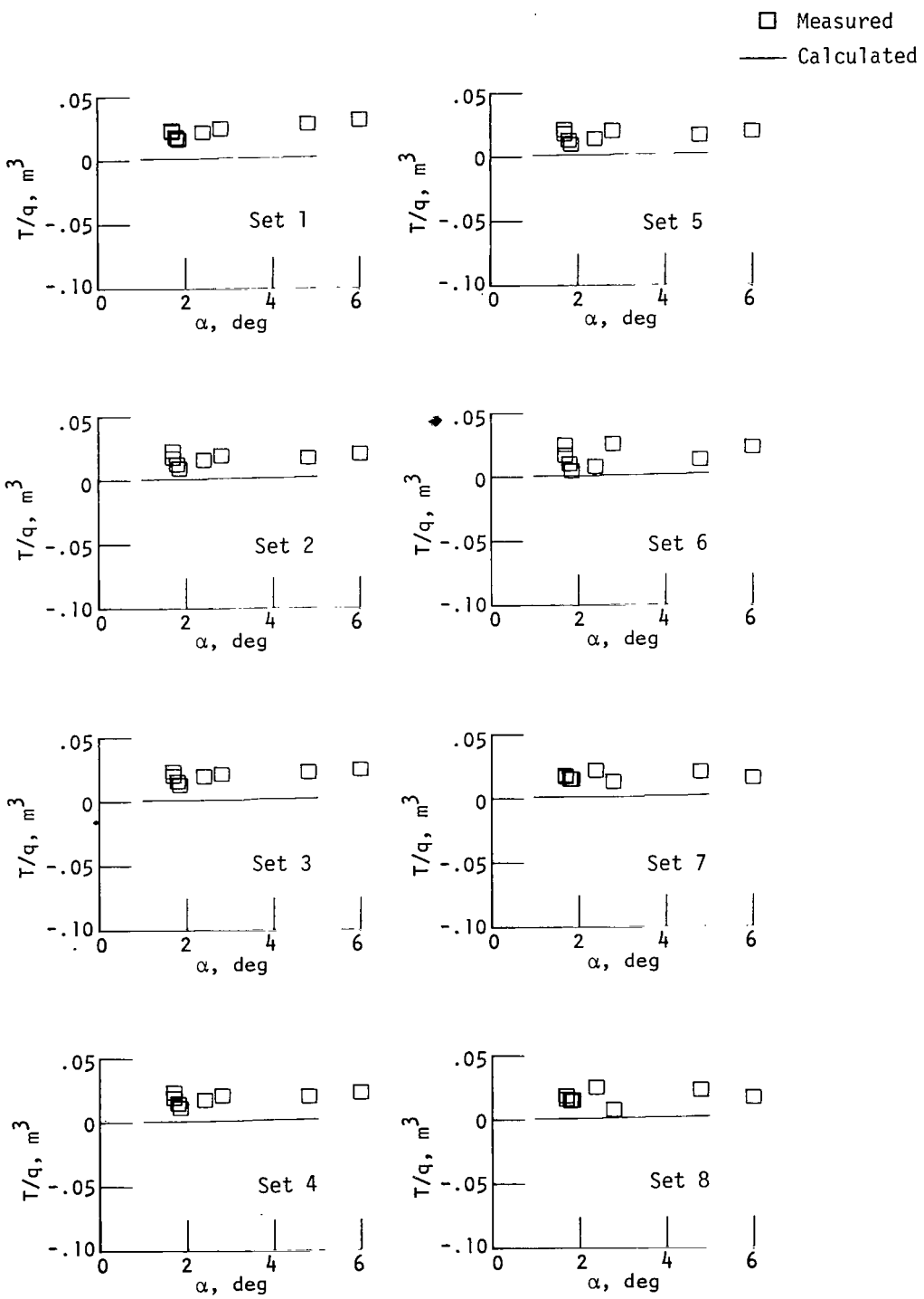

(d) Torque data for subsonic flight, tank-on configuration.

Figure 11.- Continued.

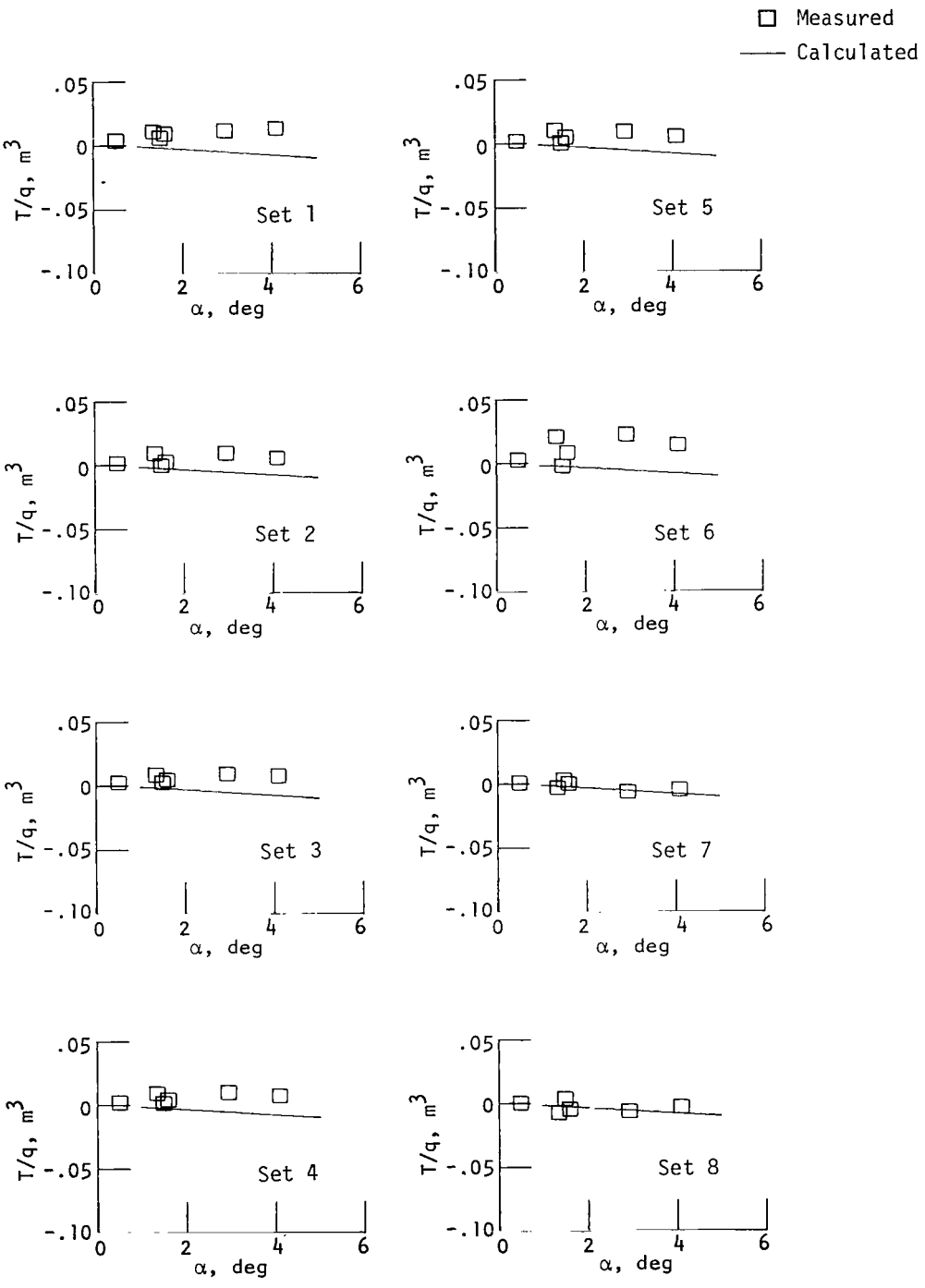

(e) Torque data for supersonic flight, tank-off configuration.

Figure 11.- Continued.

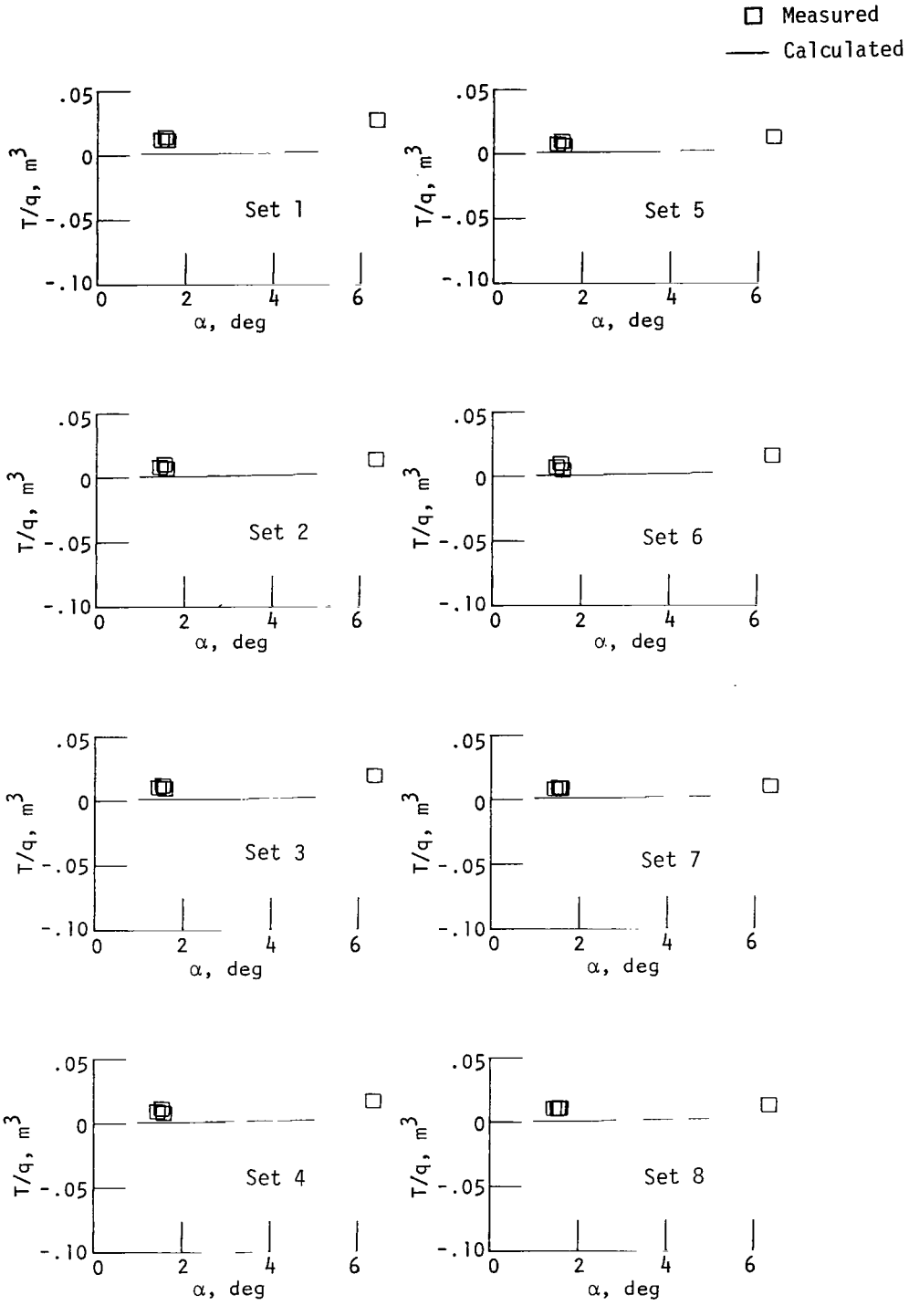

(f) Torque data for subsonic flight, tank-off configuration.

Figure 11.- Continued.

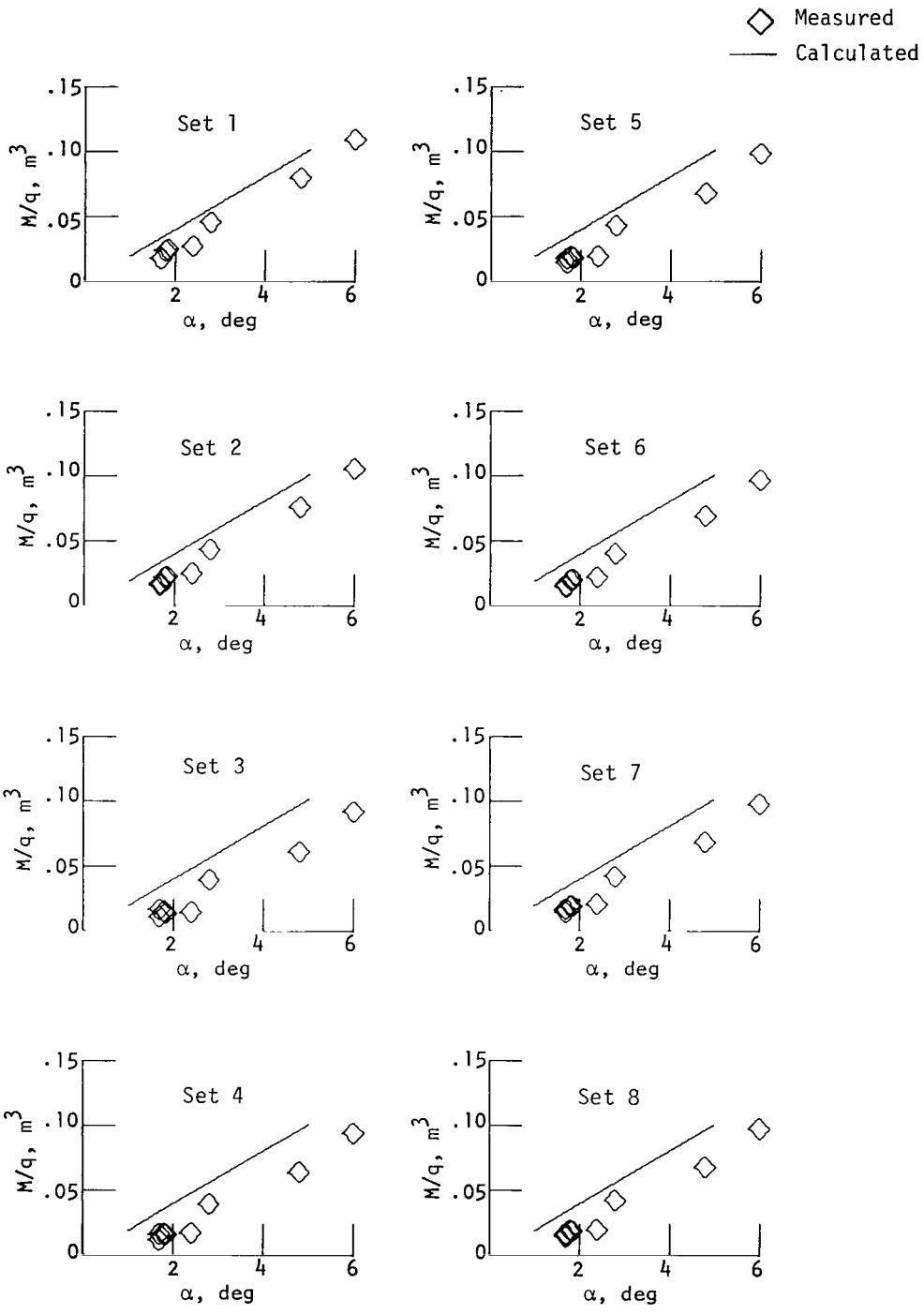

(g) Moment data for subsonic flight, tank-on configuration.

Figure 11.- Continued.

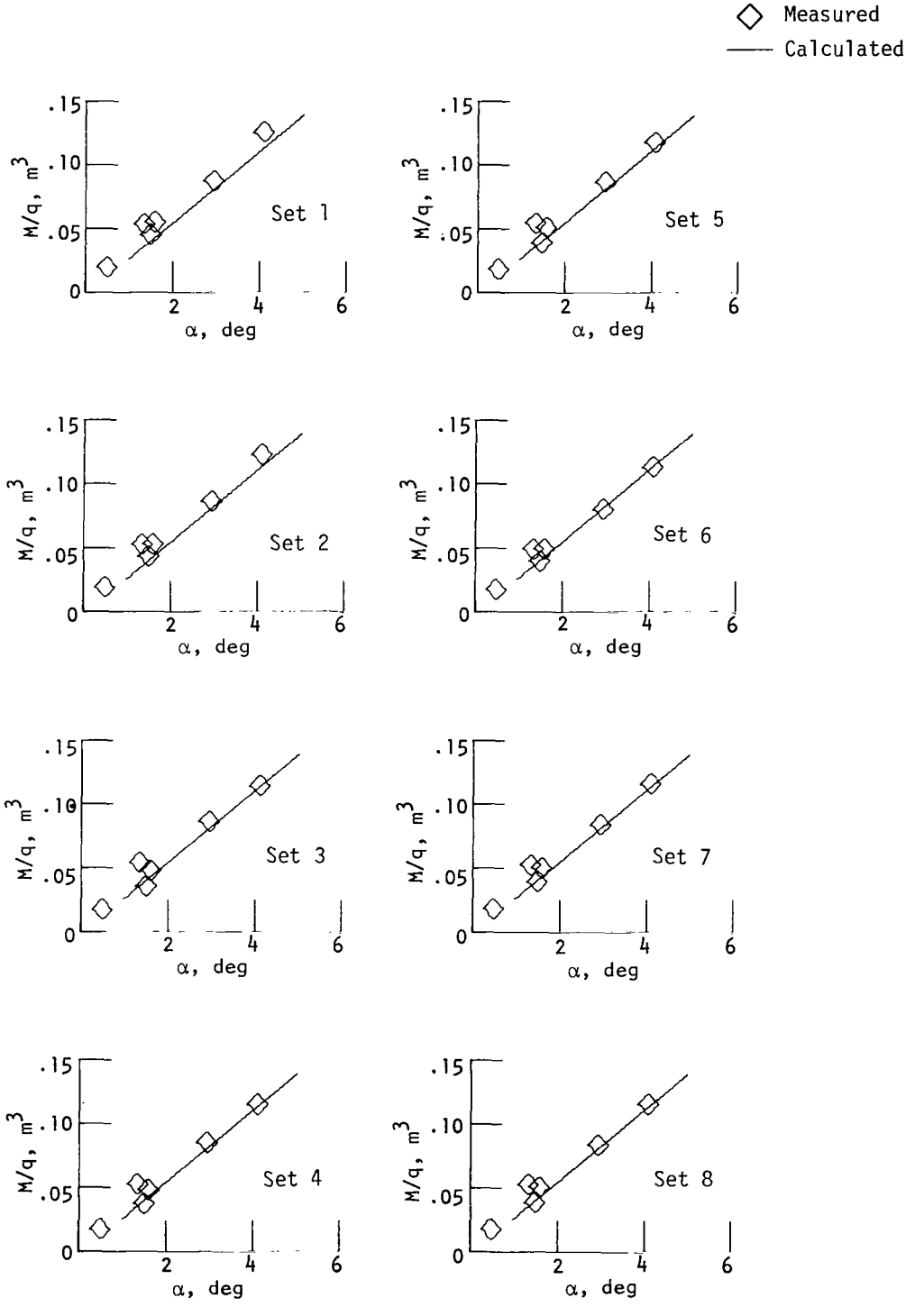

(h) Moment data for supersonic flight, tank-off configuration.

Figure 11.- Continued.

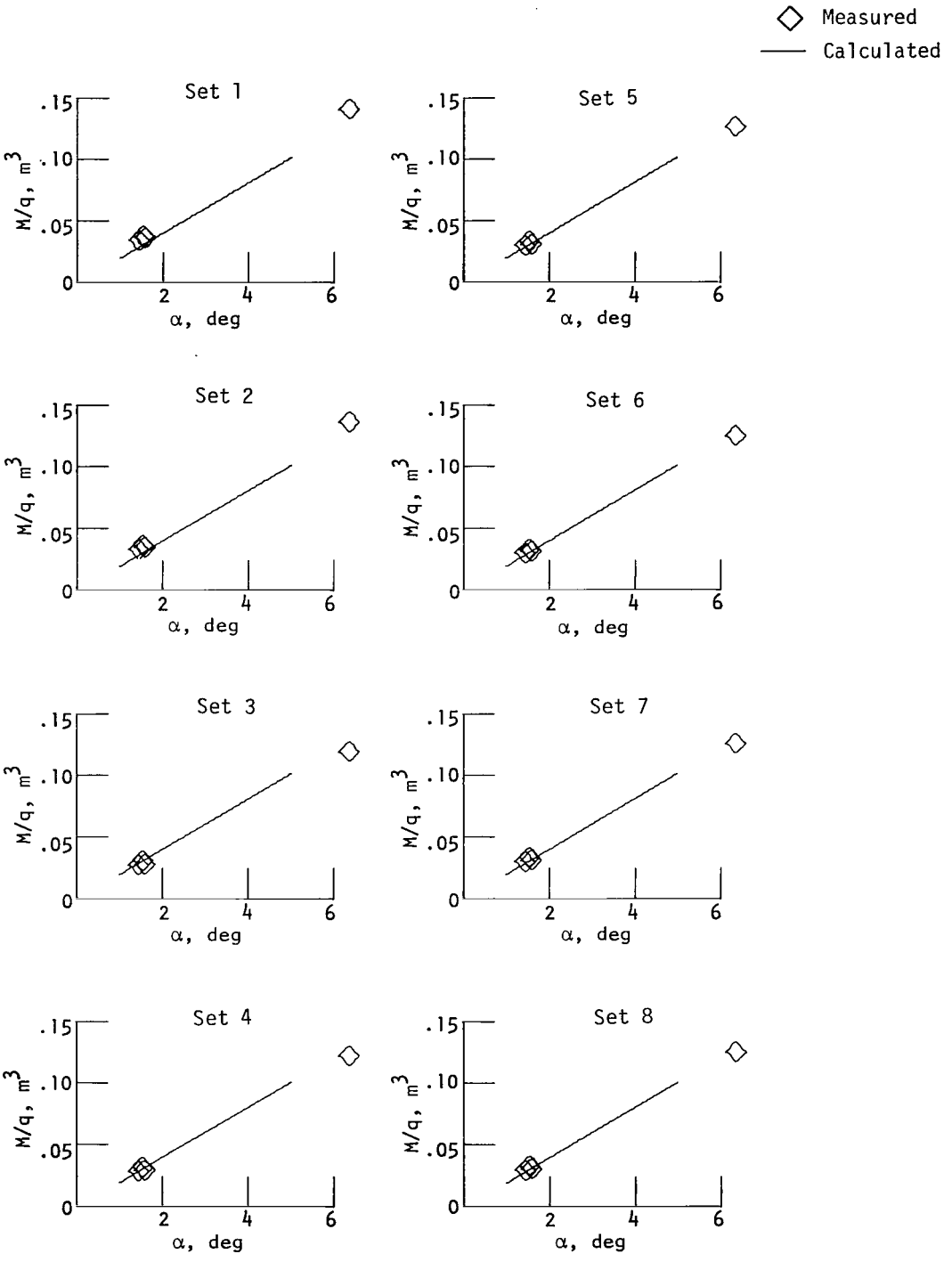

(i) Moment data for subsonic flight, tank-off configuration.

Figure 11.- Concluded.

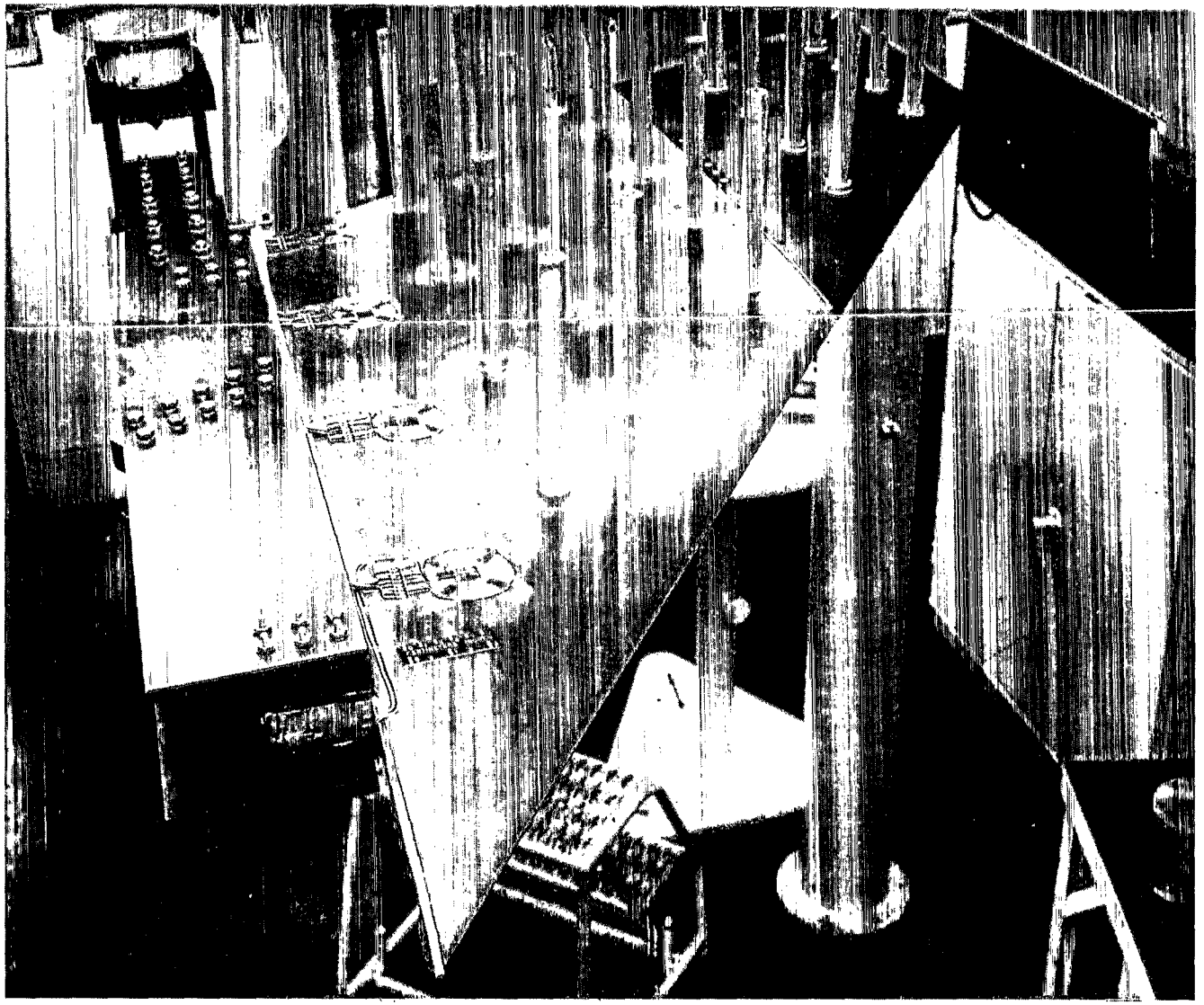

L-72-2635

Figure 12.- Strain-gage bridges on the vertical fin.

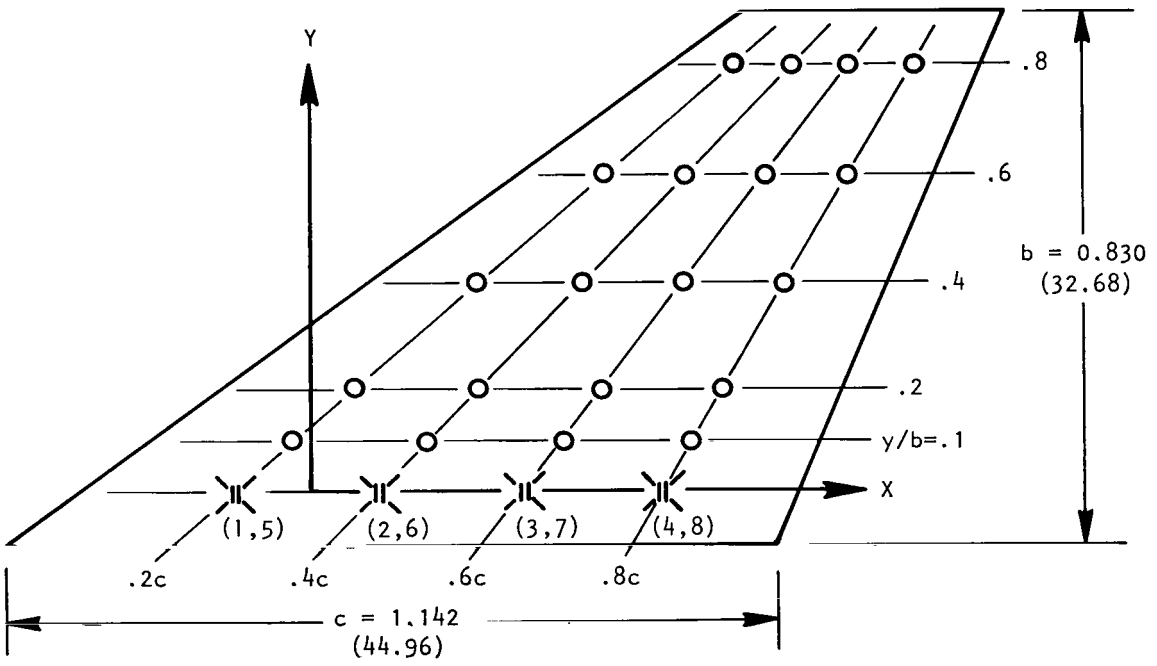

Figure 13.- Location of vertical fin strain-gage bridges and calibration load points. Dimensions are in m (in.).

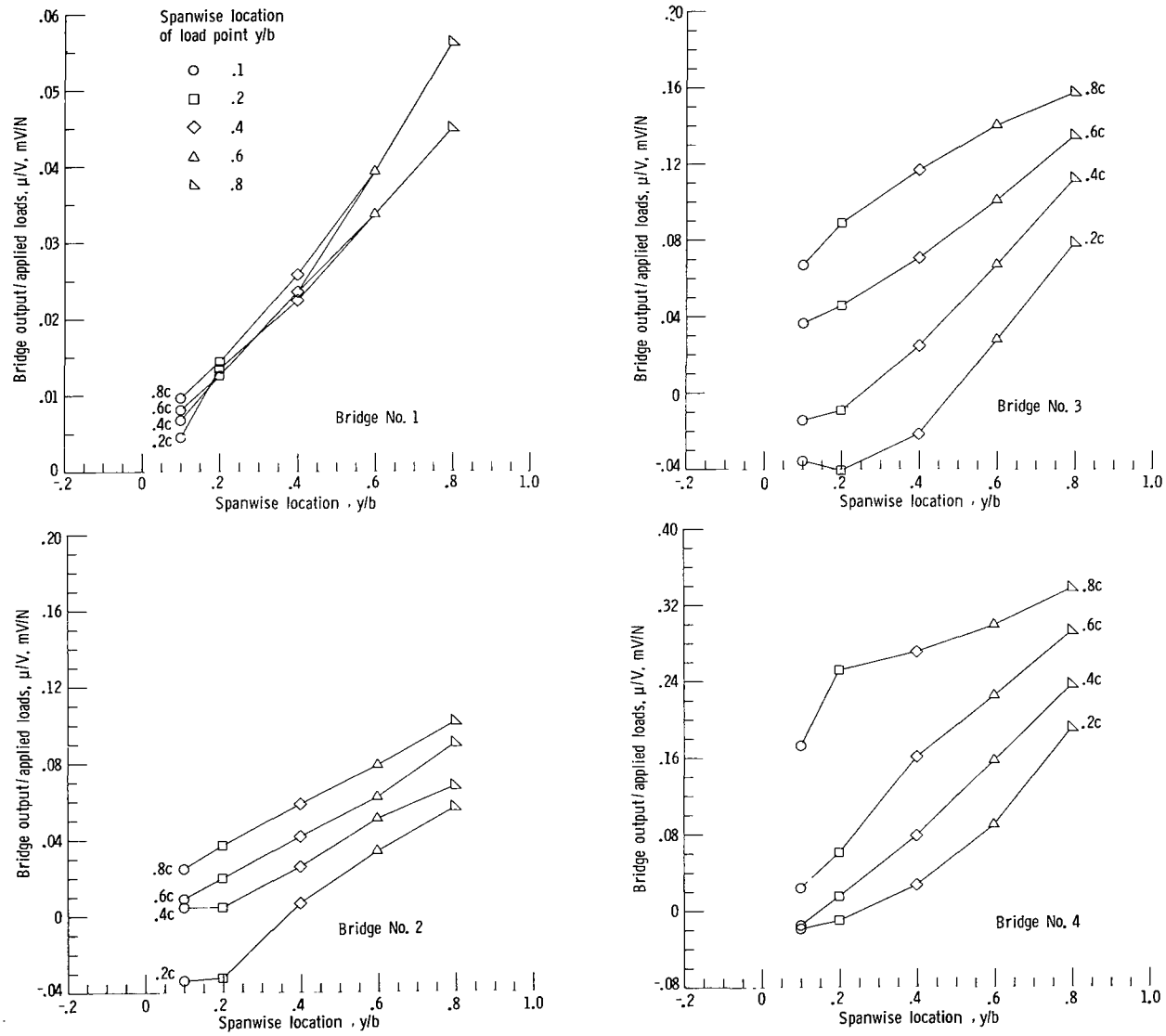

(a) Influence coefficients μ/v as a function of y/b.

Figure 14.- Influence coefficients for the vertical fin.

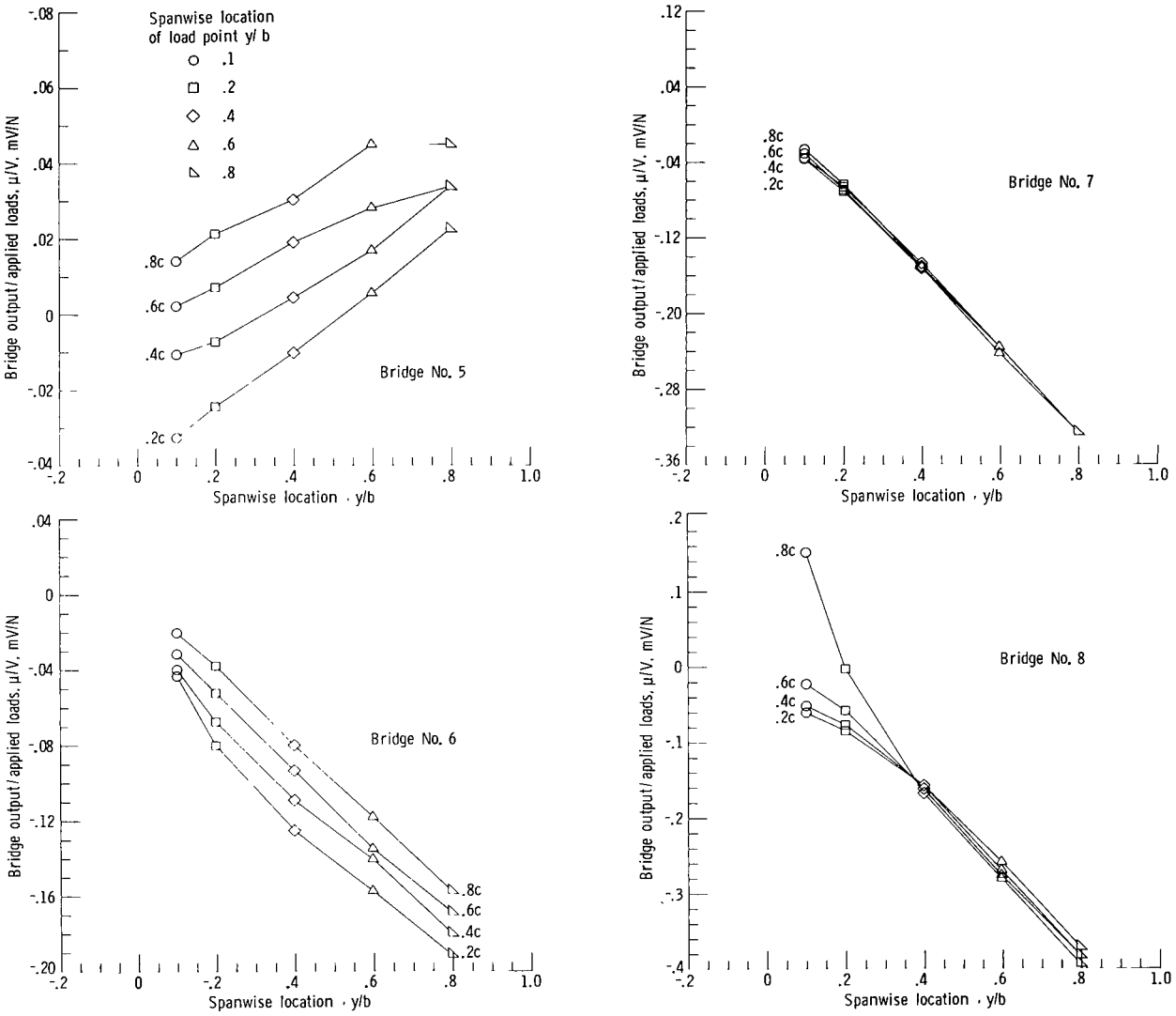

(a) Concluded.

Figure 14.- Continued.

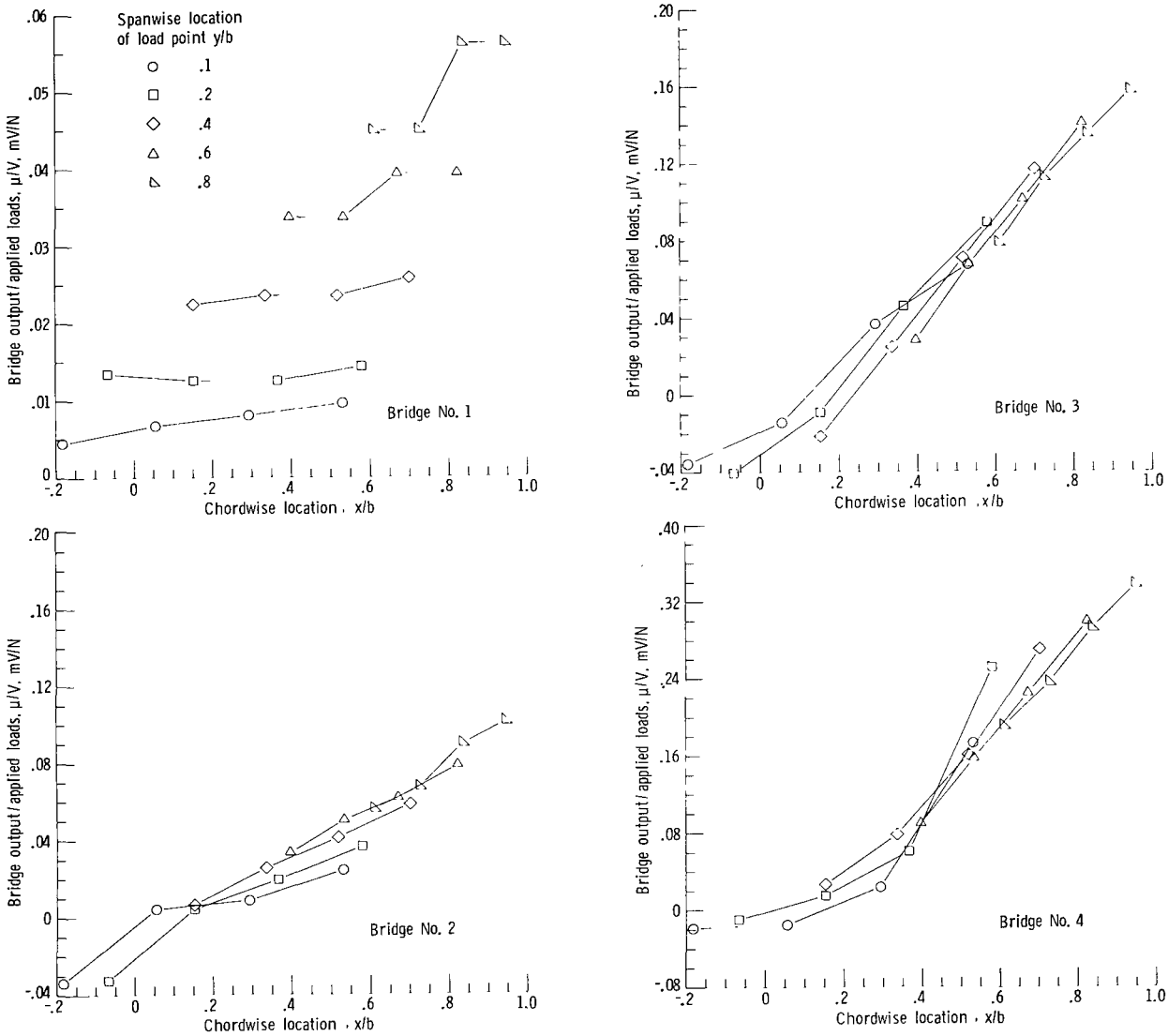

(b) Influence coefficients μ/v as a function of x/b.

Figure 14.- Continued.

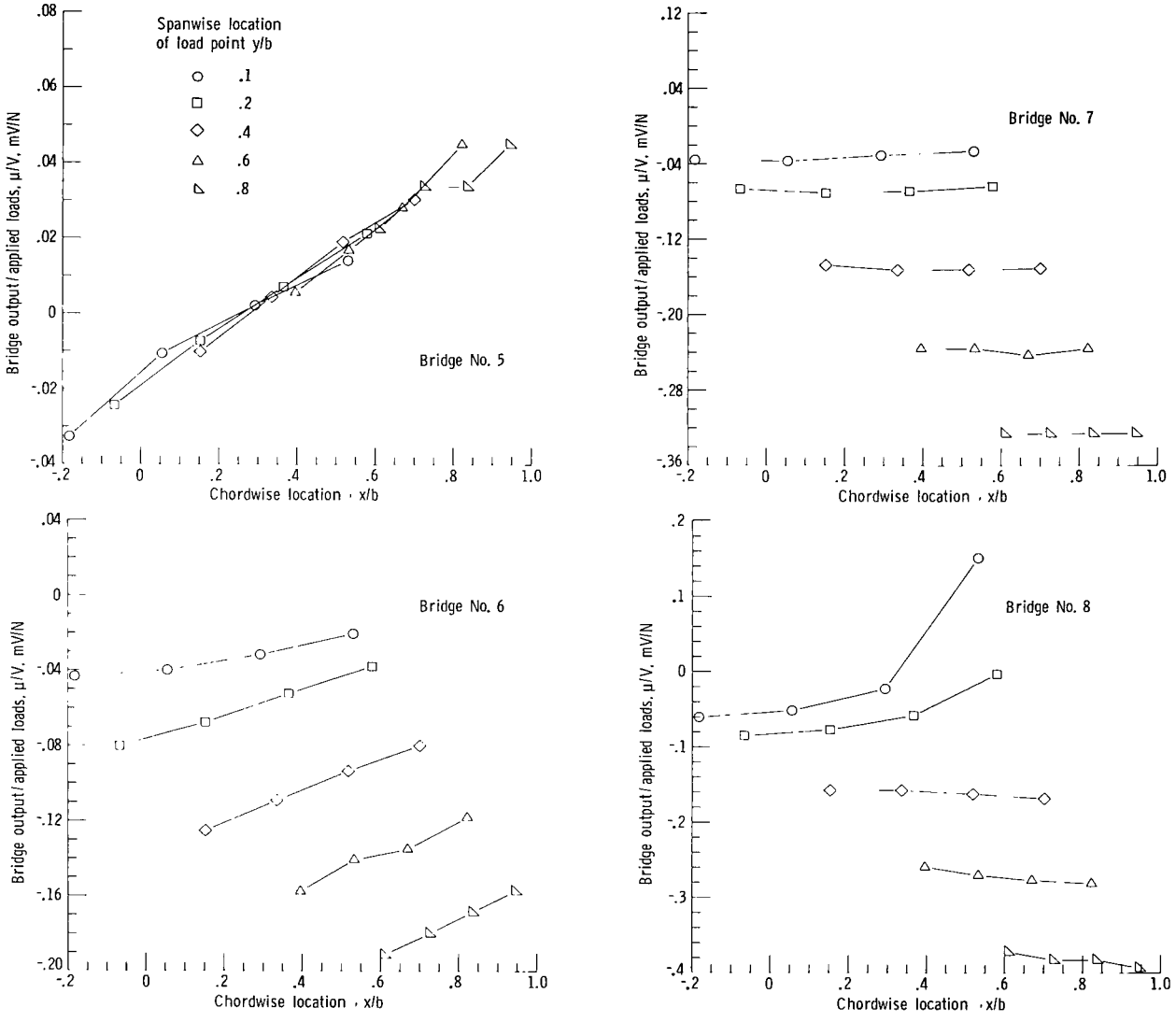

(b) Concluded.

Figure 14.- Concluded.

NATIONAL AERONAUTICS AND SPACE ADMINISTRATION
WASHINGTON, D.C. 20546

OFFICIAL BUSINESS
PENALTY FOR PRIVATE USE $300

SPECIAL FOURTH-CLASS RATE
BOOK

POSTAGE AND FEES PAID
NATIONAL AERONAUTICS AND
SPACE ADMINISTRATION
451

U.S.MAIL

"The aeronautical and space activities of the United States shall be conducted so as to contribute . . . to the expansion of human knowledge of phenomena in the atmosphere and space. The Administration shall provide for the widest practicable and appropriate dissemination of information concerning its activities and the results thereof."

—NATIONAL AERONAUTICS AND SPACE ACT OF 1958

NASA SCIENTIFIC AND TECHNICAL PUBLICATIONS

TECHNICAL REPORTS: Scientific and technical information considered important, complete, and a lasting contribution to existing knowledge.

TECHNICAL NOTES: Information less broad in scope but nevertheless of importance as a contribution to existing knowledge.

TECHNICAL MEMORANDUMS: Information receiving limited distribution because of preliminary data, security classification, or other reasons. Also includes conference proceedings with either limited or unlimited distribution.

CONTRACTOR REPORTS: Scientific and technical information generated under a NASA contract or grant and considered an important contribution to existing knowledge.

TECHNICAL TRANSLATIONS: Information published in a foreign language considered to merit NASA distribution in English.

SPECIAL PUBLICATIONS: Information derived from or of value to NASA activities. Publications include final reports of major projects, monographs, data compilations, handbooks, sourcebooks, and special bibliographies.

TECHNOLOGY UTILIZATION PUBLICATIONS: Information on technology used by NASA that may be of particular interest in commercial and other non-aerospace applications. Publications include Tech Briefs, Technology Utilization Reports and Technology Surveys.

Details on the availability of these publications may be obtained from:

SCIENTIFIC AND TECHNICAL INFORMATION OFFICE

NATIONAL AERONAUTICS AND SPACE ADMINISTRATION

Washington, D.C. 20546